MARMARA UNIVERSITY

FACULTY OF ENGINEERING

# Investigation of the Environmental Impact of a Kalina Cycle: Relationships Among Greenhouse Gas Emissions, System Performance, Turbine Inlet Temperature and Mass Flow Rate of the Working Fluid

EDA İLAYDA AFŞARKOCA

ALKAS BERK YILDIZ

NİHAL BULUT

**GRADUATION PROJECT REPORT**

Department of Mechanical Engineering

**Supervisor**

Doç. Dr. Candeniz Seçkin

ISTANBUL, 2025

MARMARA UNIVERSITY

FACULTY OF ENGINEERING

# Investigation of the Environmental Impact of a Kalina Cycle: Relationships Among Greenhouse Gas Emissions, System Performance, Turbine Exit Temperature and Mass Flow Rate of the Working Fluid

by

Eda İlayda Afşarkoca, Nihal Bulut, Alkas Berk Yıldız

July 9, 2025, Istanbul

**SUBMITTED TO THE DEPARTMENT OF MECHANICAL ENGINEERING IN PARTIAL FULFILLMENT OF THE REQUIREMENTS FOR THE DEGREE**

**OF**

**BACHELOR OF SCIENCE**

**AT**

**MARMARA UNIVERSITY**



Signature of Author(s) .....

Department of Mechanical Engineering

Certified By.....

Project Supervisor, Department of Mechanical Engineering

Accepted By.....

Head of the Department of Mechanical Engineering

## ACKNOWLEDGEMENT

This thesis has been more than an academic obligation. It has become a meaningful chapter in our lives, reflecting both personal growth and intellectual resilience.

In the early stages of our undergraduate journey, thermodynamics felt abstract and at times disheartening. It was a subject we struggled to connect with, often questioning whether we would ever fully grasp it. That perception began to change under the guidance of Assoc. Prof. Dr. Candeniz Seçkin. Her clarity, patience, and trust in our potential fundamentally reshaped our approach to learning. With her support, confusion gave way to understanding, and what once felt distant became genuinely engaging.

She was not only a supervisor. but also a mentor, a steady compass, and, in difficult moments, a source of quiet strength that helped us stay on course. Her sincere guidance, the care she showed in every correction, and the confidence she placed in us left a lasting impact not just on this thesis but on who we are becoming as engineers.

Completing a study centered on thermodynamic analysis is a fulfilling conclusion to a journey we once hesitated to begin. This work stands as a quiet testament to the transformative influence of great teaching. What she offered extended far beyond equations and cycles. She taught with heart, integrity, and an unwavering belief in our growth. These lessons will stay with us long after graduation, shaping how we think, lead, and contribute. Just as energy transitions from one form to another, we too have transformed throughout this process. Writing this thesis, the final step in our mechanical engineering education, has given us a chance to reflect on how far we have come.

During this journey, we encountered challenges in coursework, personal setbacks, and moments when our motivation waned. Yet each of those experiences helped shape the ground we now stand on, bringing us to this moment with greater clarity and strength. If our lives were a book, this would be the final page of a significant chapter. What comes next is not an end, but the beginning of something new. We move forward with excitement, shaped by this journey and deeply grateful for everyone who was part of it

**July, 2025** **Eda İlayda Afşarkoca, Nihal Bulut, Alkas Berk Yıldız**

# CONTENTS

## ABSTRACT

This study investigates the thermodynamic and environmental performance of a Kalina Cycle driven by biomethane obtained from the anaerobic digestion of food waste. The aim is to evaluate how key operating parameters such as the working fluid mass flow rate and the turbine inlet temperature affect both energy efficiency and greenhouse gas emissions. Thermodynamic modeling was carried out using Engineering Equation Solver (EES) software to simulate component-level energy balances under varying operating conditions.

The working fluid mixture of ammonia and water was selected for its suitability in low to medium temperature applications. Emissions of $CO_2$, $CH_4$, $N_2O$, $NH_3$, and $H_2S$ were estimated through stoichiometric analysis, taking into account both the anaerobic digestion and combustion stages. For a comprehensive environmental assessment, emission-specific performance indicators were developed, expressing net power output and thermal efficiency per unit mass of emitted gas.

Additionally, the study presents an economic evaluation of $CO_2$ and $N_2O$ mitigation strategies. $CO_2$ capture was analyzed using a calcium looping process, while $N_2O$ removal was modeled through catalytic decomposition with a cobalt-based zeolite catalyst. Annual costs were estimated based on chemical usage, capture efficiencies, and energy requirements.

Overall, the results demonstrate that the Kalina Cycle can be a viable waste to energy option when integrated with emission control measures, providing both environmental and energy benefits under optimized operational conditions.$N_2O$ mitigation through carbon capture and thermal decomposition methods

## SYMBOLS

**E:** total energy content (kj)

**$\dot{Q}$:** rate of heat transfer (kW)

**$\dot{W}$:** power (kW)

**$\dot{m}$:** mass flow rate (kg/s)

**$\dot{n}$:** molar flow rate (mol/s)

**$\dot{V}$:** volumetric flow rate ($m^3/s$)

**h:** specific enthalpy (kj/kg)

**V:** velocity (m/s)

**g:** gravitational acceleration ($m/s^2$)

**z:** elevation (m)

**$\dot{Q}$:** rate of heat transfer (kW)

**°C**: celcius degree

**Δ:** change in quantity

**x :** mass fraction

**η :** efficiency

**T :** temperature (C°)

**P :** pressure (kPa)

**q:** quality

**s :** entropy (kJ/K)

**1**, **2**, **3** ... , **12 :** number of state-points in Fig. 2

**$x_p$:** Fresh CaO make-up ratio

**€:** Euro

**M**: molar mass

## SUBSCRIPTS

**in:** input

**out:** output

**is:** isentropic

**net:** net

**th:** thermal

**cap:** capture

## ABBREVIATIONS

**EES:** Engineering Equation Solver

**GHG:** Greenhouse Gas

**LTR:** Low Temperature Recuperator

**HVAC:** Heating, Ventilating and Air Conditioning

**HTR:** High Temperature Recuperator

**KC:** Kalina Cycle

**OPEX:** Operational Expenditures

**CAPEX:** Capital Expenditures

**O&M:** Operation and Maintenance

**Wh:** Watt-hour

**kWh:** kilowatt-hour

**CaL:** Calcium Looping

**Co-ZSM-5:** Cobalt-exchanged Zeolite Socony Mobil–5

**wt :** weight

**HHV:** Higher Heating Value

**LHV:** Lower Heating Value

## LIST OF FIGURES

## LIST OF TABLES

# 1. INTRODUCTION

Sustainable energy technologies have become increasingly important due to rising global awareness about climate change, resource depletion, and environmental degradation. In this context, engineering research has shifted toward developing thermodynamic systems that can efficiently convert low to medium temperature heat into useful energy with minimal environmental impact. One of the promising approaches is the Kalina Cycle, which uses a binary working fluid composed of ammonia and water. This system offers higher second-law efficiency than conventional single-fluid cycles by allowing non-isothermal phase changes. However, its environmental performance remains insufficiently explored, especially when operated with renewable fuels such as biomethane. This chapter introduces the problem, outlines the objective of the study, presents the relevant literature, and identifies the specific contribution made by this research.

The Kalina Cycle is a closed thermodynamic system that utilizes an ammonia and water mixture as the working fluid. Unlike pure substances, this mixture undergoes phase change over a range of temperatures, which improves heat transfer and reduces irreversibilities during energy conversion. As a result, the system becomes more suitable for low and medium temperature sources (Kalina, 1983; Wang et al., 2019).

Although the Kalina Cycle has been applied in geothermal and industrial waste heat recovery systems, its integration with renewable fuels such as biomethane has not been adequately investigated from an environmental perspective. Biomethane can be obtained through the anaerobic digestion of food waste and used as a combustion-based heat source. However, this process releases multiple gases including carbon dioxide, methane, nitrous oxide, ammonia, and hydrogen sulfide. These gases differ significantly in their global warming potential and health effects. For instance, nitrous oxide has a warming potential nearly 300 times greater than carbon dioxide (IPCC, 2006), and even small amounts of ammonia or hydrogen sulfide may cause local environmental damage (Seçkin, 2013).

This study aims to assess both the thermodynamic and environmental performance of a Kalina Cycle powered by biomethane derived from the anaerobic digestion of food

waste. The effects of turbine inlet temperature and working fluid mass flow rate on net power output and thermal efficiency are examined. Additionally, energy generation is compared with the amount of each emitted gas to evaluate environmental effectiveness. The feasibility of post-combustion carbon dioxide capture using calcium looping and nitrous oxide reduction through catalytic decomposition is also investigated (Abanades et al., 2002; da Cruz et al., 1998).

## 1.1 Literature Review

The Kalina Cycle was developed to improve the thermal performance of power generation systems by using a binary mixture instead of a pure fluid. Its ability to match variable heat source profiles makes it suitable for applications involving waste heat, geothermal energy, and biomass combustion (Kalina, 1983; Wang et al., 2019; Seçkin, 2020).

Anaerobic digestion is a well-known process for producing methane-rich biogas from organic waste. The Buswell equation is commonly used to estimate gas output based on the elemental composition of the input material (De Clercq, 2015). While methane serves as the primary fuel, the process also produces non-energy gases such as ammonia and hydrogen sulfide, especially when nitrogen and sulfur are present in the feedstock.

Environmental concerns related to these emissions have gained attention in recent years. Carbon dioxide and methane are standard greenhouse gases, but nitrous oxide has a far higher warming potential. Ammonia and hydrogen sulfide, although not greenhouse gases, have significant ecological and health impacts (IPCC, 2006; Seçkin, 2013). Understanding how these gases behave under different cycle conditions is critical for responsible system design.

To reduce greenhouse gas emissions, technologies such as calcium looping and catalytic decomposition have been investigated. Calcium looping captures carbon dioxide using reversible reactions between calcium oxide and calcium carbonate, with heat recovery potential from the calciner stage (Abanades et al., 2007; Romeo et al., 2008). Nitrous oxide can be decomposed into harmless nitrogen and oxygen using zeolite catalysts like Co-ZSM-5, which function effectively at moderate temperatures without requiring additional reagents (da Cruz et al., 1998; Haber et al., 2004).

Many studies have focused on the thermodynamic modeling of the Kalina Cycle, particularly its energy efficiency. However, few have addressed its environmental impact when operated with renewable combustion-based fuels. In addition, most existing work does not evaluate the cost or feasibility of emission reduction techniques. This study fills that gap by integrating performance analysis, gas-specific emission evaluation, and mitigation cost modeling into a unified framework. The results provide practical insights for implementing low-emission waste-to-energy systems using Kalina Cycle technology.

# 2. THERMODYNAMIC ANALYSIS OF KALINA CYCLE

The KC is a closed thermodynamic system designed to convert thermal energy into mechanical work by utilizing a binary mixture of ammonia and water as the working fluid (Wang et al., 2019). The fundamental analytical basis of this process is the First Law of Thermodynamics, which governs the energy transformations taking place within each component of the system (Çengel and Boles, 2015). In the context of steady-flow control volumes, this law asserts that the energy entering a control volume must equal the energy leaving it, accounting for heat transfer, work interactions, and the enthalpy associated with mass flow (Çengel and Boles, 2015).

For the system considered in this study, which is modeled under steady-state conditions, variations in kinetic and potential energies are assumed to be negligible when compared to changes in enthalpy. Consequently, the energy equation simplifies to a form that relates heat input, work output, and the enthalpy change between the inlet and outlet of each component. This approach facilitates a systematic component-level analysis of the KC and allows for the calculation of key performance indicators such as net power generation and thermal efficiency.

Each component within the cycle, ranging from the heat exchangers and separator to the turbine, recuperators, condenser, and pump, has been evaluated individually in terms of its thermodynamic role. The interactions of heat, mass, and energy between the inlet and outlet state points were carefully assessed to determine their contribution to the overall cycle behaviour. Particular attention was paid to the changes in enthalpy, pressure, temperature, entropy, and ammonia mass fraction throughout the cycle, as these properties directly influence energy conversion efficiency.

The thermodynamic model employed in this study is structured around twelve distinct state points, each of which represents a transition in the condition of the working fluid. The relationships among these points, along with the governing energy balances, form the basis for calculating the system's total work output and efficiency. This methodology enables a comprehensive evaluation of how the cycle performs under varying operating parameters and serves as the foundation for the environmental and economic analyses presented in the subsequent chapters.

## 2.1 First Law of Thermodynamics for Steady-Flow Control Volumes

The First Law of Thermodynamics states that energy can neither be created nor destroyed; it can only be transferred or transformed (Çengel and Boles, 2015). When applied to an open system (a control volume where mass crosses the boundary) this law is used to track how energy in various forms (such as heat, work, and mass flow) moves through the system.

For a control volume, the energy balance over a time interval is given as:

$$E_{in} - E_{out} = \Delta E_{system} \tag{2.1}$$

This equation simply states:

"The net energy transferred into the system is equal to the change in energy stored within the system."

In the context of an engineering system operating under steady-state conditions, properties such as temperature, pressure, and mass flow rate do not change with time at any point in the system. Therefore, the amount of energy stored within the system remains constant (Çengel and Boles, 2015). Mathematically, this implies:

$$\Delta E_{system} = 0 \tag{2.2}$$

And the energy balance simplifies to:

$$E_{in} = E_{out} \tag{2.3}$$

Since;

$$E = m\left(h + \frac{V^2}{2} + gz\right) \tag{2.4}$$

Then in rate form, considering continuous flows of mass and energy, this becomes:

$$\dot{Q} - \dot{W} = \sum_{out} \dot{m}\left(h + \frac{V^2}{2} + gz\right) - \sum_{in} \dot{m}\left(h + \frac{V^2}{2} + gz\right) \tag{2.5}$$

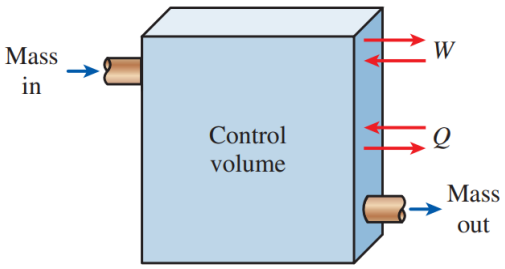


**Figure 2.1**: Control volume schematic illustrating energy and mass interactions.

In continuous flow systems, this equation is frequently used in rate form, allowing for real-time energy flow analysis. The terms in the equation represent the following: $\dot{Q}$ indicates the rate of heat transfer into or out of the control volume, such as thermal energy supplied by a combustor or absorbed in a heat exchanger; $\dot{W}$ denotes the rate of mechanical work done by or on the control volume, corresponding to shaft work generated in turbines or energy consumed by pumps; and $h_{in}$ and $h_{out}$ refer to the specific enthalpy of the working fluid at the inlet and outlet, respectively, encapsulating both internal energy and the flow work associated with mass movement (Çengel and Boles, 2015).

$$\dot{Q} - \dot{W} = \dot{m}(h_{out} - h_{in}) \tag{2.6}$$

This simplified version, commonly known as the steady-flow energy equation, is widely applied in the thermodynamic analysis of power systems. It emphasizes the most influential term, the change in enthalpy, while typically neglecting kinetic and potential energy variations, which are usually minor compared to enthalpy differences in components such as turbines, pumps, and heat exchangers (Çengel and Boles, 2015).

In most thermal power systems, including the KC, variations in fluid velocity and elevation are small and have limited impact on energy balances. Therefore, the terms

associated with kinetic energy $\frac{V^2}{2}$ and potential energy gz are justifiably omitted. However, in applications involving significant speed or elevation differences, such as in jet propulsion or hydroelectric systems, these contributions must be retained for accurate analysis (Çengel and Boles, 2015).

Energy enters and exits control volumes through several pathways. Heat may be transferred by conduction, convection, or radiation. Work is exchanged in mechanical or electrical form. Enthalpy is transported with the mass flow of the fluid. All of these interactions are present in the KC. Thermal energy generated from combustion is transferred to the working fluid via the heat exchanger, work is extracted in the turbine and supplied to the pump, and the binary mixture carries enthalpy throughout the cycle.

The simplified form of the First Law for steady-flow systems provides a practical framework for evaluating the energy behaviour of each component in the KC. By applying this principle to the individual subsystems, one can accurately quantify heat input, mechanical work output, and fluid energy transport, which enables a complete performance evaluation of the overall power generation cycle.

## 2.2 System Overview and Component-Level Thermodynamic Analysis

The KC examined in this study operates as a closed-loop thermodynamic system using a binary working fluid composed of ammonia and water. This mixture, owing to its variable boiling behaviour, enables effective energy extraction from low- to medium-grade heat sources (Wang et al., 2019). The system includes a set of interconnected components that convert thermal energy into mechanical work while ensuring internal energy conservation through regenerative heat exchange.

The configuration adopted in this analysis is illustrated in Figure 2, where twelve distinct thermodynamic state points define the entry and exit conditions of each component. These points form the basis for the calculation of energy and mass balances throughout the system. The main components include the heat exchanger, separator, turbine, high-temperature and low-temperature recuperators (HTR and LTR), condenser, expansion valve, and pump. Each of these plays a critical thermodynamic role in

maintaining the cycle's energy continuity and overall efficiency.

Thermal energy enters the cycle through the heat source, where the ammonia–water mixture is subjected to the heat generated by biomethane combustion. As this binary fluid absorbs heat, a portion of it transitions into vapor. Due to the distinct boiling points of the two components, ammonia having a significantly lower boiling point than water, ammonia tends to vaporize first. This selective vaporization is a key advantage of using an ammonia–water mixture: it allows the cycle to operate effectively at lower temperatures compared to single-component working fluids (Kalina, 1983; Wang et al., 2019).

The resulting two-phase mixture is then directed to the separator, where the vapor and liquid phases are split based on their differences in density and composition. The lighter, ammonia-rich vapor rises and is extracted as the upper stream, while the denser, water-rich liquid settles as the lower stream. This phase separation ensures that high-quality vapor enters the turbine, allowing efficient energy conversion into mechanical work.

The ammonia-rich vapor, carrying high thermal energy, passes through the turbine. Inside the turbine, this thermal energy is converted into mechanical work as the vapor drives the turbine blades, producing rotational motion that can be harnessed as shaft work. After exiting the turbine, the vapor becomes part of the returning stream that merges with the liquid stream exiting the bottom of the separator. Before the mixture is condensed, it passes through two recuperative heat exchangers (HTR and LTR) which are essential for maintaining internal energy recovery (Seçkin, 2020; Wang et al., 2019).

The purpose of HTR and LTR is to reduce the thermal load on the condenser by transferring energy within the cycle itself. These recuperators operate by utilizing the temperature gradient between adjacent fluid streams in separate flow paths. The high-temperature stream from the turbine and separator provides heat to the colder, pressurized working fluid returning from the pump. This internal heat exchange minimizes the amount of energy rejected to the environment through the condenser, thereby reducing the need for additional external heat input in the subsequent cycle. In the absence of these recuperators, a larger quantity of heat would be discharged through the condenser during each cycle, and to maintain cycle continuity, a greater amount of external heat would have

to be supplied repeatedly (Wang et al., 2019). Therefore, HTR and LTR not only enhance energy efficiency but also promote thermal sustainability by limiting unnecessary losses.

The liquid-rich stream from the separator passes through the HTR, where it transfers energy to the incoming cold stream in the opposite pipe, facilitated by the existing temperature difference. Following this process, the stream is routed to the expansion valve, where its pressure is adjusted to match that of the turbine outlet. This isenthalpic process ensures pressure equilibrium without altering the specific enthalpy of the flow.

After the expansion valve, the liquid stream merges with the vapor exiting the turbine. The combined stream then enters the LTR, where it gives up additional heat to the cold fluid that was previously pressurized by the pump. This secondary internal heat exchange further reduces the thermal burden on the condenser and improves the overall thermal utilization of the cycle (Kalina, 1983; Wang et al., 2019).

The mixed stream eventually reaches the condenser, where residual heat is rejected to the surroundings. The fluid is then transformed into a saturated liquid state and proceeds to the pump. In this component, mechanical work is applied to increase the pressure of the working fluid, preparing it for re-entry into the heat exchanger. After pressurization, the fluid once again passes through the LTR and HTR, where it absorbs previously recovered internal energy before arriving at the heat exchanger to begin a new cycle.

The thermodynamic properties, including temperature, pressure, enthalpy, entropy, and ammonia concentration, are monitored across all state points. These values are used to evaluate the behaviour of each component and the system as a whole. Under the assumption of ideal and steady-state operation, this section provides the basis for quantifying component-level energy exchanges and supports the subsequent performance

and emission analyses presented in this study.

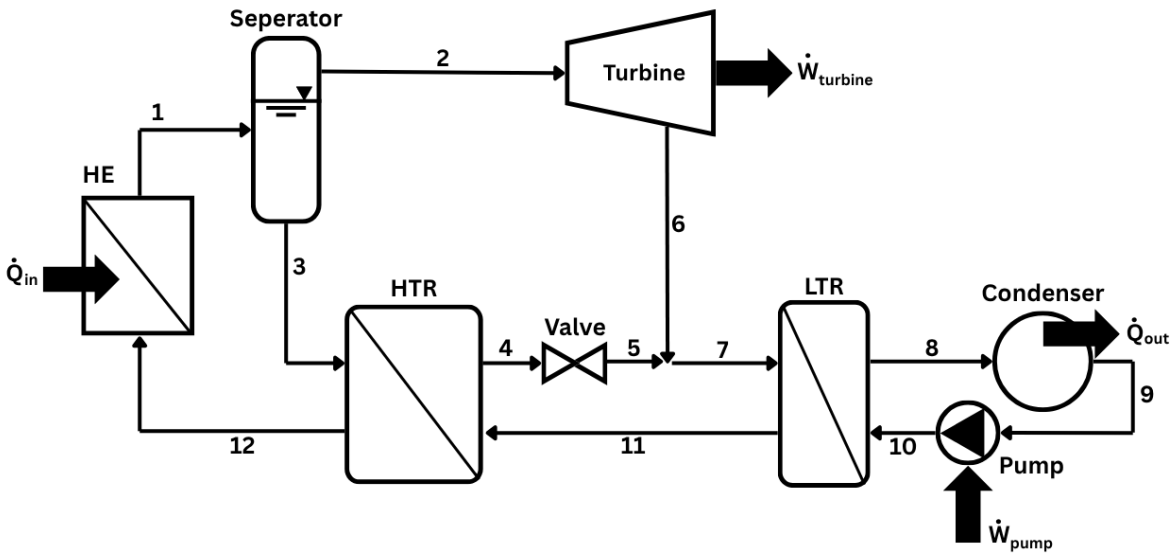


**Figure 2.2:** Schematic representation of the Kalina cycle configuration analyzed in this study, showing the key components and numbered state points for thermodynamic evaluation.

### 2.2.1 Heat Exchanger

The heat exchanger, also referred to as the vapor generator, is the component in which external thermal energy is transferred to the working fluid, initiating the power conversion process of the KC. In this system, the source of heat is derived from the combustion of biomethane. The binary mixture of ammonia and water enters the heat exchanger at state point 12 as a pressurized liquid and absorbs thermal energy through a heat exchanger. As a result of this energy input, the fluid undergoes a partial or complete phase change, exiting the heat exchanger at state point 1.

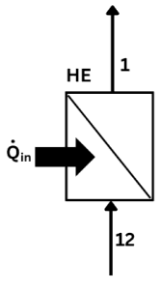

**Figure 2.3:** Diagram of a heat exchanger with inlet 12 and outlet 1.

The process can be modeled under steady-flow conditions by applying the First Law of Thermodynamics. Assuming negligible changes in kinetic and potential energy and the absence of shaft work, the energy balance across the heat exchanger is expressed as:

$$\dot{Q}_{in} = \dot{m}_1(h_1 - h_{12}) \tag{2.7}$$

Here, $\dot{Q}_{in}$ represents the rate of thermal energy transferred from the combustion source, $\dot{m}_1$ is the mass flow rate of the working fluid, $h_{12}$ is the specific enthalpy at the inlet, and $h_1$ is the specific enthalpy at the outlet of the heat exchanger. The entire enthalpy increase is attributed to the heat absorbed by the working fluid as it changes phase from liquid to vapor (Çengel and Boles, 2015).

One of the defining characteristics of the KC is the non-isothermal vaporization behaviour of the ammonia–water mixture. Unlike a pure substance, the mixture does not boil at a constant temperature; instead, it experiences a temperature glide due to the varying saturation properties of its components. This enables a better thermal match with the heat source, reducing irreversibilities and enhancing the overall cycle efficiency (Kalina, 1983; Wang et al., 2019).

At the outlet of the heat exchanger, the fluid exists as a high-temperature, high-pressure two-phase mixture. The vapor content, rich in ammonia, is lighter than the accompanying liquid, which contains a higher concentration of water. This condition facilitates the physical separation of the mixture in the next component, the separator. The vapor phase, having absorbed significant thermal energy, is prepared for expansion in the turbine, while the liquid phase will later contribute to internal heat recovery.

### 2.2.2 Seperator

The separator is a critical component in the KC, responsible for dividing the two-phase mixture exiting the heat exchanger into ammonia-rich vapor and water-rich liquid streams. This thermodynamic separation is essential for ensuring that high-quality vapor, suitable for expansion, is directed toward the turbine, while the remaining liquid phase

can be utilized in internal heat recovery processes.

Upon entering the separator at state point 1, the working fluid exists as a pressurized, high-temperature mixture composed of vapor and liquid phases. The separation mechanism relies on differences in both density and composition. As the mixture resides within the separator, the vapor phase naturally rises due to its lower density and higher ammonia content, while the heavier, water-rich liquid phase settles at the bottom. This phase behaviour is consistent with the thermodynamic properties of the ammonia–water mixture, wherein ammonia exhibits a significantly lower density and boiling point compared to water (Kalina, 1983; Wang et al., 2019). Additionally, the higher volatility of ammonia causes it to concentrate in the vapor phase during boiling, further enhancing the quality of the vapor stream.

The vapor stream, enriched in ammonia and thermal energy, is extracted from the top of the separator and routed to the turbine for expansion and work generation. In contrast, the liquid stream, which contains a reduced concentration of ammonia, is directed toward the HTR, where it contributes to internal energy recovery through regenerative heat exchange.

The separator does not involve any external heat or work interaction and is modeled as an adiabatic component operating under steady-flow conditions. The primary energy interaction occurs through the redistribution of enthalpy between the two streams according to mass and composition balance. The total mass and energy must be conserved across the separator, which is expressed through the following relations:

$$\dot{m}_1 = \dot{m}_2 + \dot{m}_3 \tag{2.8}$$

$$\dot{m}_1 * x_1 = \dot{m}_2 * x_2 + \dot{m}_3 * x_3 \tag{2.9}$$

$$\dot{m}_1 * h_1 = \dot{m}_2 * h_2 + \dot{m}_3 * h_3 \tag{2.10}$$

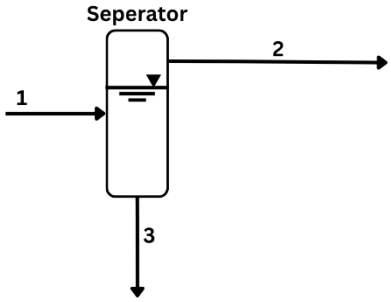


**Figure 2.4:** A diagram of a seperator.

In these equations, $\dot{m}_1$ is the mass flow rate entering the separator, while $\dot{m}_2$ and $\dot{m}_3$ represent the vapor and liquid outlet flow rates, respectively. The symbols x denotes ammonia mass fraction which is the the proportion of ammonia in the ammonia–water working fluid and h denotes specific enthalpy at the respective state points.

$$x = \frac{m_{NH_3}}{m_{NH_3} + m_{H_2O}} \tag{2.11}$$

where $m_{NH_3}$ is the mass of ammonia and $m_{H_2O}$ is the mass of water in the mixture. The value of x ranges between 0 and 1, where $x = 1$ indicates pure ammonia and $x = 0$ corresponds to pure water. Mass fraction is a critical parameter in determining the thermodynamic behaviour of the binary fluid throughout the cycle (Kalina, 1983).

The efficiency of the separation process has a direct influence on the performance of downstream components. A well-separated, ammonia-rich vapor stream maximizes the energy extracted by the turbine, while a water-rich liquid stream enhances the effectiveness of the recuperators by providing a stable thermal gradient.

### 2.2.3 Turbine

The turbine is the primary work-producing component of the KC. It receives high-pressure, ammonia-rich vapor from the separator at state point 2 and expands this vapor to a lower pressure level, resulting in mechanical shaft work. This conversion of thermal energy into kinetic energy and then into mechanical work is central to the power generation objective of the cycle (Wang et al., 2019).

As the vapor enters the turbine, it possesses high enthalpy and relatively low density. The expansion process reduces its pressure and temperature, causing a corresponding drop in enthalpy. The kinetic energy of the expanding vapor is transferred to the turbine blades, which rotate and generate useful work. The fluid exits the turbine at state point 6, now at a reduced pressure and partially condensed.

The energy balance for the turbine is formulated by applying the First Law of Thermodynamics to a control volume under steady-flow conditions. Neglecting heat loss to the surroundings and assuming negligible changes in kinetic and potential energy, the specific turbine work output is expressed as:

$$\dot{W}_{turbine} = \dot{m}_2(h_2 - h_6) \tag{2.12}$$

However, since the actual expansion process is not perfectly isentropic due to mechanical and thermodynamic irreversibilities, the isentropic efficiency of the turbine must be considered. The actual outlet enthalpy $h_6$ is calculated from the isentropic enthalpy $h_{6is}$ and turbine efficiency $\eta_{turbine}$, as shown below:

$$\eta_{turbine} = \frac{h_2 - h_6}{h_2 - h_{6is}} \tag{2.13}$$

$$h_6 = h_2 - \eta_{turbine} * (h_2 - h_{6is}) \tag{2.14}$$

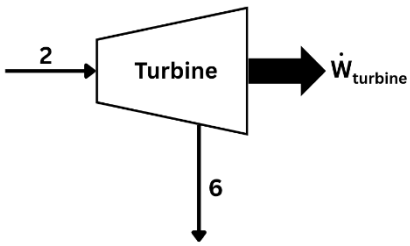


**Figure 2.5:** A diagram of a turbine.

Here, $h_{6is}$ is obtained assuming isentropic expansion from state point 2 to the turbine exit pressure, and $\eta_{turbine}$ is the isentropic efficiency of the turbine, typically less than unity. The work output from the turbine is therefore dependent not only on the pressure ratio and enthalpy drop but also on the quality of the incoming vapor and the thermodynamic properties of the ammonia–water mixture (Kalina, 1983; Çengel and

Boles, 2015).

Following expansion, the vapor exiting the turbine contains less energy and is partially condensed. This stream later merges with the liquid stream exiting the bottom of the separator. Together, they proceed through the LTR, where they contribute to internal heat recovery before reaching the condenser.

### 2.2.4 High Temperature Recuperator

The HTR is a key component that enhances the thermal efficiency of the KC by enabling internal energy recovery. It functions as a counterflow heat exchanger that allows thermal energy to be transferred from a hotter stream within the cycle to a cooler one, without involving any external heat source or sink. This internal regeneration reduces the amount of heat that would otherwise be lost to the surroundings and lowers the external thermal input required to sustain the cycle (Wang et al., 2019; Çengel and Boles, 2015).

In the present configuration, the hot fluid entering the HTR at state point 3 is the liquid-rich stream exiting the bottom of the separator. This stream contains considerable residual thermal energy. On the opposite side of the heat exchanger, the cold working fluid enters at state point 11. This fluid has been pressurized by the pump and has just exited the LTR. The temperature difference between these two streams facilitates heat transfer, raising the enthalpy of the cold stream while reducing that of the hot stream.

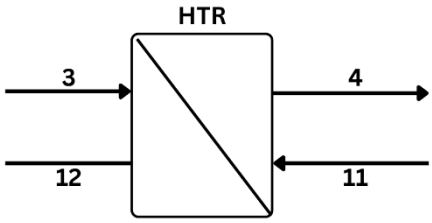


**Figure 2.6:** A diagram of a high temperature recuperator.

The heat exchange that occurs in the HTR is modeled under steady-flow and adiabatic assumptions. No mass is exchanged between the two channels, and the process is treated as internally reversible. The energy balance for the hot and cold sides is given by the following expressions:

$$\dot{Q}_{HTR} = \dot{m}_3(h_3 - h_4) \tag{2.15}$$

And also

$$\dot{Q}_{HTR} = \dot{m}_{11}(h_{11} - h_{12}) \tag{2.16}$$

Meaning the two expressions are equal;

$$\dot{m}_3(h_3 - h_4) = \dot{m}_{11}(h_{11} - h_{12}) \tag{2.17}$$

Here, $\dot{m}_3$ and $\dot{m}_{11}$ are the respective mass flow rates, and h values denote the specific enthalpies at the inlet and outlet of each stream. The thermal energy extracted from the hot stream is thus equal to the energy gained by the cold stream, assuming ideal conditions.

The use of the HTR significantly reduces the thermal load on the condenser by recovering part of the heat that would otherwise be released to the environment. Consequently, the external heat input required in the next cycle is decreased, resulting in improved overall thermal efficiency. Without the HTR, the energy carried by the separator's liquid outlet would be entirely discharged through the condenser, necessitating greater external heat input to maintain the same cycle output (Wang et al., 2019; Kalina, 1983).

Furthermore, by preheating the working fluid before it enters the heat exchanger, the HTR enhances thermal compatibility during the vaporization process. This improves the temperature gradient match between the heat source and the working fluid, reduces entropy generation, and increases the second-law efficiency of the cycle (Çengel and Boles, 2015).

### 2.2.5 Valve

The expansion valve in the KC is a throttling device that serves to reduce the pressure of the working fluid without producing work or requiring energy input. Its primary function is to ensure pressure equalization between the liquid stream exiting the HTR and the low-pressure side of the cycle following the turbine outlet. This pressure adjustment enables the mixing of fluid streams at compatible conditions and ensures smooth progression through subsequent components, particularly the LTR and the

condenser.

In this system configuration, the expansion valve receives the liquid-rich stream at state point 4, which has passed through the HTR and possesses relatively high pressure. The valve reduces the pressure to the level of the turbine outlet (state point 5) through an isenthalpic process, meaning that the enthalpy of the fluid remains constant during the pressure drop (Çengel and Boles, 2015). The process can be described by the following relation:

$$h_4 = h_5 \tag{2.18}$$

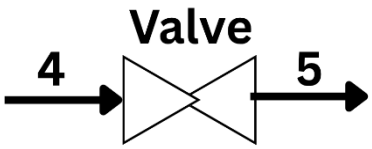


**Figure 2.7:** A diagram of a valve.

This expression indicates that while the pressure decreases across the valve, there is no change in the fluid's specific enthalpy. However, the temperature typically decreases as a result of the throttling, and in some cases, partial vaporization may occur due to the sudden drop in pressure, depending on the thermodynamic state of the fluid.

The expansion valve does not contribute to any energy recovery or production within the cycle. Instead, it performs a necessary control function that enables proper pressure matching and phase stability. The presence of this component also simplifies system design by avoiding the need for more complex mechanical expansion devices in the liquid flow path.

Following the expansion process, the fluid at state point 5 merges with the stream exiting the turbine at state point 6. This combined stream continues toward the LTR, where further internal heat exchange takes place.

### 2.2.6 Low Temperature Recuperator

The LTR is the second regenerative heat exchanger in the KC and plays a key role in conserving internal energy by further reducing the thermal load on the condenser. After the expansion process and turbine exit, two fluid streams, one from the expansion valve

(state point 5) and one from the turbine outlet (state point 6), merge and form a combined stream that enters the LTR at state point 7. This mixture typically has a lower enthalpy and temperature compared to the working fluid leaving the pump at state point 10, which has already been pressurized.

The LTR facilitates heat exchange between these two streams. The relatively hot mixture at state point 7 releases part of its residual thermal energy to the colder, pressurized working fluid entering the LTR at state point 10. As a result, the mixed stream is cooled and leaves the LTR at state point 8, while the pump outlet stream is preheated and exits the LTR at state point 11, before continuing to the HTR.

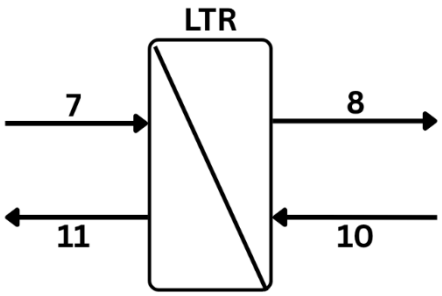


**Figure 2.8:** A diagram of a low temperature recuperator.

The energy balances across the LTR can be written as follows:

$$\dot{Q}_{LTR} = \dot{m}_7(h_7 - h_8) \tag{2.19}$$

And also

$$\dot{Q}_{LTR} = \dot{m}_{10}(h_{11} - h_{10}) \tag{2.20}$$

Meaning the two expressions are equal;

$$\dot{m}_7(h_7 - h_8) = \dot{m}_{10}(h_{11} - h_{10}) \tag{2.21}$$

These expressions represent the heat released by the mixture flowing from the turbine and expansion line, and the corresponding heat absorbed by the pump outlet stream. Under the assumption of ideal heat exchange and no losses to the surroundings, the heat transferred from one stream is equal to the heat gained by the other (Wang et al., 2019).

The use of the LTR provides multiple benefits. First, it ensures that some of the

residual energy within the cycle is reused rather than being wasted in the condenser. This not only enhances energy utilization but also reduces the rate of heat rejection to the environment. Second, by preheating the working fluid before it reaches the HTR, the LTR contributes to improved thermal matching, resulting in a more gradual and efficient heat absorption profile during vaporization. Lastly, it reduces the demand for external fuel input over multiple cycles, thereby increasing both the thermal and environmental performance of the system (Kalina, 1983; Wang et al., 2019).

### 2.2.7 Condenser

The condenser is the component in which the working fluid rejects its remaining thermal energy to the environment. This heat removal process lowers the temperature and enthalpy of the fluid, bringing it to a saturated liquid state required for subsequent pressurization by the pump. While the condenser does not involve mechanical work or chemical transformation, it plays a critical role in ensuring the stability and continuity of the thermodynamic cycle (Çengel and Boles, 2015).

After passing through the HTR and LTR, the working fluid enters the condenser at state point 8. At this point, the fluid may exist as a two-phase mixture or a subcooled liquid, depending on the preceding heat exchange conditions. Within the condenser, the fluid comes into thermal contact with an external cooling medium, such as air or water, and transfers its residual heat. As a result, the fluid exits the condenser at state point 9 in a saturated liquid state.

The heat rejected in the condenser is quantified by the following energy balance:

$$\dot{Q}_{out} = \dot{m}_8(h_8 - h_9) \tag{2.22}$$

where $\dot{Q}_{out}$ out is the rate of heat transfer to the environment, $\dot{m}_8$ is the mass flow rate of the working fluid, and $h_8$ and $h_9$ are the specific enthalpies at the condenser inlet and outlet, respectively.

The main function of the condenser is to remove heat that cannot be utilized internally and to condition the fluid for the pump. Proper condensation is essential to prevent vapor entry into the pump, which could lead to cavitation and mechanical failure. The condenser ensures that the fluid enters the pump as a stable saturated liquid,

maintaining both operational safety and performance (Çengel and Boles, 2015).

In KC configurations with internal regeneration, the condenser typically handles a reduced thermal load because a significant portion of the fluid's energy has already been recovered by the recuperators. This improves system efficiency, reduces the required cooling capacity, and minimizes environmental impact (Wang et al., 2019).

### 2.2.8 Pump

The pump is the component responsible for increasing the pressure of the working fluid from the condenser outlet conditions to the pressure required at the inlet of the heat addition process. By supplying mechanical work to the system, the pump enables the continuation of the thermodynamic cycle and ensures that the working fluid re-enters the regenerative heat exchangers in a pressurized liquid state (Çengel and Boles, 2015).

In the KC configuration examined in this study, the working fluid enters the pump at state point 9 as a saturated liquid. The pump increases the pressure without significant heat exchange, and the fluid exits at state point 10. This process is modeled under steady-flow conditions, assuming negligible changes in kinetic and potential energy. The mechanical work input required by the pump is calculated using the following relation:

$$\dot{W}_{pump} = \dot{m}_9(h_{10} - h_9) \tag{2.23}$$

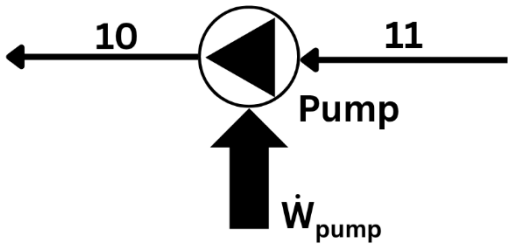


**Figure 2.9:** A diagram of a pump.

Since real pumps are not perfectly efficient, the isentropic efficiency of the pump must be taken into account. The actual outlet enthalpy $h_{10}$ is determined by using the isentropic enthalpy $h_{10s}$ and the pump efficiency $\eta_{pump}$, according to:

$$\eta_{pump} = \frac{h_{10s} - h_9}{h_{10} - h_9} \tag{2.24}$$

Here, $\eta_{pump}$ represents the isentropic efficiency of the pump, and $h_{10s}$ is the enthalpy the fluid would have if the compression were isentropic (Çengel and Boles, 2015).

The pump does not alter the phase of the working fluid; it remains in the liquid state throughout the process. However, the pressure increase is essential for allowing the fluid to effectively absorb heat in the recuperators and the heat exchanger. If the pump does not provide sufficient pressure, the working fluid may not reach the necessary thermodynamic conditions to complete vaporization in the heat exchanger (Çengel and Boles, 2015).

Following pressurization, the fluid continues to state point 10 and enters the LTR, where it begins to recover energy internally from other parts of the cycle. This preheating step improves thermal matching, enhances efficiency, and reduces the external heat input required in the heat exchanger (Wang et al., 2019).

## 2.3 Net Power Generation and Thermal Efficiency

The performance of the KC is evaluated through two principal thermodynamic metrics: net power output and thermal efficiency. These values indicate how effectively the cycle converts supplied heat into useful mechanical work and how much of that work remains after accounting for internal energy consumption. All calculations are based on the steady-flow form of the First Law of Thermodynamics, applied to individual components of the cycle (Çengel and Boles, 2015).

### 2.3.1 Turbine Work Output

The mechanical power generated by the turbine is calculated from the enthalpy drop of the working fluid as it expands from the high-pressure turbine inlet (state 2) to the lower-pressure outlet (state 6):

$$\dot{W}_{turbine} = \dot{m}_2(h_2 - h_6) \tag{2.25}$$

Since the expansion process is not perfectly isentropic, the actual outlet enthalpy $h_6$ is calculated using the isentropic efficiency of the turbine and the ideal enthalpy $h_{6is}$:

$$\eta_{turbine} = \frac{h_2 - h_6}{h_2 - h_{6is}} \tag{2.26}$$

$$h_6 = h_2 - \eta_{turbine} * h_2 - h_{6is} \tag{2.27}$$

Here, $h_{6is}$ represents the enthalpy the fluid would have if the expansion were isentropic. In this study, the turbine efficiency is taken as 0.80.

### 2.3.2 Pump Work Input

The pump increases the pressure of the saturated liquid exiting the condenser (state 9), enabling it to re-enter the heat input section at a higher pressure (state 10). The power consumed by the pump is given by:

$$\dot{W}_{pump} = \dot{m}_9(h_{10} - h_9) \tag{2.28}$$

As the pumping process is not ideal, the actual outlet enthalpy $h_{10}$ is determined using the isentropic enthalpy $h_{10s}$ and the pump efficiency:

$$\eta_{pump} = \frac{h_{10s} - h_9}{h_{10} - h_9} \tag{2.29}$$

In this analysis, the pump efficiency is assumed to be 0.60. This correction accounts for losses due to internal friction and fluid dynamics within the pump (Çengel and Boles, 2015).

### 2.3.3 Net Power Output

The net power output of the cycle is obtained by subtracting the pump work input from the turbine work output:

$$\dot{W}_{net} = \dot{W}_{turbine} - \dot{W}_{pump} \tag{2.30}$$

This value represents the actual mechanical power available for useful external applications, such as electrical generation or mechanical drive systems.

### 2.3.4 Thermal Efficiency

The thermal efficiency of the KC expresses how effectively the system converts heat input into net mechanical power. It is calculated as:

$$\eta_{th} = \frac{\dot{W}_{net}}{\dot{Q}_{in}} \tag{2.31}$$

The heat input to the system is defined by the energy absorbed in the vapor generator:

$$\dot{Q}_{in} = \dot{m}_1(h_1 - h_{12}) \tag{2.32}$$

The values of $\dot{W}_{net}$ and $\eta_{th}$ form the baseline for evaluating the cycle's energetic performance. In subsequent sections, these metrics will be analyzed under different operating conditions such as changes in mass flow rate ($\dot{m}_1$), turbine inlet temperature ($T_2$), and ammonia concentration. Their correlation with environmental parameters, including greenhouse gas emissions, will also be investigated (Wang et al., 2019).

To connect thermodynamic performance with environmental impact, the following indicators are used:

*Net Power per Unit Emission:*

$$\frac{\dot{W}_{net}}{\dot{m}_{gas}} \quad \left[\frac{kW}{\frac{mg}{s}}\right] \tag{2.33}$$

This ratio indicates how many kilowatts of useful power are produced per milligram per second of a specific gas emitted.

*Thermal Efficiency per Unit Emission:*

$$\frac{\eta_{th}}{\dot{m}_{gas}} \quad \left[\frac{-}{\frac{mg}{s}}\right] \tag{2.34}$$

This expression reflects the thermal efficiency attributed to each milligram per second of gas released (Wang et al., 2019).

# 3. KALINA CYCLE MODELING

In this study, the Engineering Equation Solver (EES) software was utilized to perform the thermodynamic modeling and energy-emission analysis of the KC. EES is a

powerful numerical tool developed for solving nonlinear algebraic and differential equations commonly encountered in thermal-fluid sciences. Its built-in library includes extensive thermophysical property data for a wide range of substances, including ammonia–water mixtures, making it particularly well-suited for advanced cycle simulations (F-Chart Software, 2023).

The complete thermodynamic model of the KC, including all state points and component interactions (e.g., heat exchangers, separator, turbine, recuperators, condenser, and pump), was implemented within the EES environment. The software allowed for the precise calculation of enthalpy, entropy, temperature, and mass fraction values at each state, based on the provided assumptions and known input parameters.

Furthermore, EES was instrumental in determining the net power output and thermal efficiency of the system. Emission-related computations, such as greenhouse gas mass flows and performance indicators (i.e., energy or efficiency per unit emission), were also integrated into the EES code. The data required for generating performance and environmental impact graphs, such as those showing the effects of mass flow rate and turbine inlet temperature, were all obtained through systematic parametric simulations executed in EES.

The use of EES enabled consistent, accurate, and adaptable modeling, ensuring that the results reflect realistic thermodynamic behaviour and environmental implications. Its flexibility in handling iterative calculations and property interpolation made it the ideal choice for analyzing the complex interactions within the KC (F-Chart Software, 2023).

The complete set of equations and assumptions used to model the KC were implemented in the EES (Engineering Equation Solver) environment. Below is the full EES code developed for this study, which includes all thermodynamic property evaluations, mass and energy balances, component-level calculations, and emission-related computations. This code served as the computational backbone for generating the results and graphical analyses presented in this report.

## 3.1 EES Modeling

The thermodynamic modeling of the Kalina Cycle was performed using Engineering Equation Solver (EES) software, which allows for detailed state-point analysis of complex power cycles involving multicomponent working fluids. The model incorporates the fundamental conservation laws of mass, energy, and species, alongside idealized assumptions and component-level efficiency definitions. This section outlines the structure of the EES implementation, beginning with the selection of input parameters, followed by a discussion of the applied assumptions, and concluding with the governing equations used in the simulation.

### 3.1.1 Input Parameters

To perform a reliable thermodynamic analysis of the KC, several initial conditions and operating parameters must be defined. These input values are either based on standard design practices reported in the literature, selected to represent realistic working conditions, or assumed for simplification of the system model (Çengel and Boles, 2015). The parameters govern the behaviour of the working fluid at key state points and directly influence energy balances, component performance, and overall cycle efficiency.

**Table 3.1:** Summary of the input parametes used in the Kalina cycle model,including thermodynamic conditions, working fluid properties and component efficiencies applied in the simulation.

| Parameter | Symbol | Value | Unit |
|---|---|---|---|
| Heat input to the cycle | $\dot{Q}_{in}$ | 1000 | kW |
| Mass fraction of ammonia at state 1 | $x_1$ | 0.7 | – |
| Turbine isentropic efficiency | $\eta_{turbine}$ | 0.80 | – |
| Pump isentropic efficiency | $\eta_{pump}$ | 0.60 | – |
| Temperature at state 2 (Turbine inlet) | $T_2$ | 120 | °C |
| Pressure at state 1 | $P_1$ | 3500 | kPa |
| Mass flow rate of working fluid | $\dot{m}_1$ | 0.98 | kg/s |
| Quality at state 2 | $q_2$ | 1 | – |
| Quality at state 3 | $q_3$ | 0 | – |
| Quality at state 9 | $q_9$ | 0 | – |

Table 3.1 presents the baseline input values employed in the simulation. These include thermodynamic properties such as temperature, pressure, ammonia concentration, and phase quality at selected state points, as well as component-level efficiencies and mass flow rate. Certain idealized assumptions, such as constant entropy during isentropic processes or uniform ammonia composition across specific flow paths, have been introduced to ensure consistency and computational feasibility.

### 3.1.2 Assumptions

Mass Flow Continuity Assumptions:

$$\dot{m}_1 = \dot{m}_7 = \dot{m}_8 = \dot{m}_9 = \dot{m}_{10} = \dot{m}_{11} = \dot{m}_{12} \tag{3.1}$$

$$\dot{m}_2 = \dot{m}_6 \tag{3.2}$$

$$\dot{m}_3 = \dot{m}_4 = \dot{m}_5 \tag{3.3}$$

Thermodynamic Property Assumptions:

$$P_{max} = P_1 = P_2 = P_3 = P_4 = P_{10} = P_{11} = P_{12} \tag{3.4}$$

$$P_{min} = P_5 = P_6 = P_7 = P_8 = P_9 \tag{3.5}$$

$$T_1 = T_2 = T_3 \tag{3.6}$$

$$x_1 = x_7 = x_8 = x_9 = x_{10} = x_{11} = x_{12} \tag{3.7}$$

Mass flow rates are assumed to remain constant across designated segments of the cycle, eliminating the need for individual mass balance calculations within those regions.

Uniform pressure is applied to high-pressure and low-pressure sections of the system, simplifying the analysis by neglecting pressure losses across components.

Temperature at key points such as the heat exchanger outlet and both separator branches is assumed to be equal.

The turbine inlet stream is modeled as saturated vapor, while the separator's liquid outlet and condenser outlet are treated as saturated liquid to allow direct use of property tables.

Ammonia concentration is assumed to remain constant between components of KC, simplifying the treatment of composition changes in the binary mixture.

These assumptions streamline the thermodynamic analysis and are consistent with standard modeling practices in preliminary cycle evaluations (Çengel and Boles, 2015).

### 3.1.3 Functions and Equations In EES Software

This section outlines the key equations and modeling logic implemented in Engineering Equation Solver (EES) to simulate the KC. Each component is represented using steady-flow energy balances, isentropic relations, and internal heat exchange equations. These formulations enable the calculation of thermodynamic properties, system efficiency, and emission outputs under varying operating conditions.

EES uses built-in thermophysical property functions to compute state variables such

as temperature, enthalpy, entropy, and pressure for both real fluids and ideal gases. Each function begins with the name of the fluid (e.g., "NH3H2O" for an ammonia–water mixture), followed by named arguments like T=, P=, h=, or x=. As an example:

$$T = f("NH_3H_2O", P, x, h)$$

In this expression, EES retrieves the temperature by interpolating property data from its internal database, based on the given pressure, quality (mass fraction), and specific enthalpy. Argument order is flexible as long as the fluid name is placed first, and values are automatically matched to the appropriate thermodynamic tables. This structure allows for efficient cycle modeling by solving any combination of known and unknown properties using consistent, built-in relationships.

The functions used are listed below:

$$P_9 = f(T_9, x_9, q_9) \tag{3.8}$$

$$P_8 = f(T_8, x_8, h_8) \tag{3.9}$$

$$\dot{Q}_{out} = \dot{m}_8(h_8 - h_9) \tag{3.10}$$

Condenser pressure and heat rejection are determined from outlet conditions.

$$x_2 = f(T_2, P_2, q_2) \tag{3.11}$$

$$x_3 = f(T_3, P_3, q_3) \tag{3.12}$$

$$\dot{m}_1 = \dot{m}_2 + \dot{m}_3 \tag{3.13}$$

$$\dot{m}_1 * x_1 = \dot{m}_2 * x_2 + \dot{m}_3 * x_3 \tag{3.14}$$

$$\dot{m}_1 * h_1 = \dot{m}_2 * h_2 + \dot{m}_3 * h_3 \tag{3.15}$$

Mass, concentration, and energy balances are applied at the separator.

$$h_2 = f(T_2, P_2, q_2) \tag{3.16}$$

$$s_2 = f(T_2, P_2, q_2) \tag{3.17}$$

$$h_{6is} = f(P_6, x_6, s_2) \tag{3.18}$$

$$h_6 = h_2 - \eta_{turbine} * h_2 - h_{6is} \tag{3.19}$$

$$T_6 = f(P_6, x_6, h_6) \tag{3.20}$$

$$\dot{W}_{turbine} = \dot{m}_2(h_2 - h_6) \tag{3.21}$$

Isentropic efficiency is used to calculate turbine outlet enthalpy and power output.

$$h_3 = f(T_3, P_3, q_3) \tag{3.22}$$

$$h_1 = f(T_1, P_1, x_1) \tag{3.23}$$

$$\dot{Q}_{in} = \dot{m}_1(h_1 - h_{12}) \tag{3.24}$$

Heat added in the vapor generator is computed from enthalpy difference.

$$q_7 = f(P_7, x_7, s_6) \tag{3.25}$$

$$T_7 = f(P_7, x_7, q_7) \tag{3.26}$$

$$h_7 = f(T_7, P_7, x_7) \tag{3.27}$$

$$\dot{m}_7(h_7 - h_8) = \dot{m}_{10}(h_{11} - h_{10}) \tag{3.28}$$

Energy balance is applied between the hot and cold streams in the LTR.

$$h_4 = h_5 \tag{3.29}$$

$$T_4 = f(P_4, x_4, h_4) \tag{3.30}$$

$$T_7 = f(P_5, x_5, h_5) \tag{3.31}$$

Expansion through the valve is modeled as an isenthalpic process.

$$h_{11} = f(T_{11}, P_{11}, x_{11}) \tag{3.32}$$

$$\dot{m}_3(h_3 - h_4) = \dot{m}_{11}(h_{11} - h_{12}) \tag{3.33}$$

HTR transfers energy from the hot liquid stream to the colder return stream.

$$h_9 = f(T_9, P_9, x_9) \tag{3.34}$$

$$s_9 = f(T_9, P_9, x_9) \tag{3.35}$$

$$h_{10s} = f(P_{10}, x_{10}, s_9) \tag{3.36}$$

$$\dot{W}_{pump} = \dot{m}_9(h_{10} - h_9) \tag{3.37}$$

$$h_{10} = h_9 - (h_9 - h_{10s}) * \eta_{pump} \tag{3.38}$$

$$T_{10} = f(P_{10}, x_{10}, h_{10}) \tag{3.39}$$

Pump work is determined from the enthalpy rise, corrected by isentropic efficiency.

$$\dot{W}_{net} = \dot{W}_{turbine} - \dot{W}_{pump} \tag{3.40}$$

$$\eta_{th} = \frac{\dot{W}_{net}}{\dot{Q}_{in}} \tag{3.41}$$

Overall cycle performance is evaluated from net work and thermal efficiency.

# 4. EMISSION

In this section, a detailed emission analysis was conducted to evaluate the environmental outputs of the integrated system. Starting from the AD of restaurant-based food waste to the combustion of the resulting biomethane in the Kalina Cycle, all major emission components were identified, quantified, and converted into molar, mass, and volumetric flow rates. This comprehensive approach enabled the assessment of both biogenic and combustion-based emissions, forming the basis for subsequent environmental impact comparisons.

## 4.1 Buswell Equation

The increasing amount of food waste produced in urban areas presents both a challenge and an opportunity. On one hand, organic waste contributes significantly to environmental problems when left unmanaged; on the other hand, it contains valuable chemical energy that can be recovered through appropriate technologies. AD offers a well-established method for converting such waste into biogas, a renewable energy source primarily composed of methane. This process not only reduces the burden on landfills but also enables the generation of energy from materials that would otherwise be discarded.

The potential of biogas becomes particularly relevant when integrated with high-efficiency energy conversion technologies. One such system is the KC, which uses a mixture of ammonia and water as the working fluid. Thanks to this binary composition, the KC can operate efficiently with lower temperature heat sources, such as the thermal energy released from methane combustion. This makes it a strong candidate for coupling with biogas systems, especially in decentralized, small to medium scale applications.

This study focuses on the environmental aspect of such a system: the emissions resulting from the conversion of restaurant based food waste into energy via a KC configuration. The aim is to evaluate, in quantitative terms, the environmental footprint of the entire pathway, from the decomposition of food waste in an anaerobic reactor to the combustion of methane in the heat recovery unit.

To achieve this, the study applies Buswell's equation to estimate the composition of gases generated during AD based on the elemental makeup of typical food waste. These gases (including $CH_4$, $CO_2$, $NH_3$, and $H_2S$) are then quantified in terms of both molar and mass flow rates.

In order to estimate the emissions generated during the AD of food waste, the stoichiometric composition of the resulting biogas must be calculated. For this purpose, Buswell's equation was utilized, as it provides a theoretical model for predicting the gaseous outputs of AD processes based on the elemental composition of the substrate (De Clercq et al., 2016).

**Table 4.1:** Elemental composition of 1000 g of food waste.

| Element | %M/M (%g/g) | Mass (g) | Atomic Weight (g/mol) | Mass (mol) |
|---|---|---|---|---|
| C | 47.6 | 476 | 12 | 39.35 |
| H | 7.04 | 70.4 | 1 | 70.40 |
| O | 33.3 | 333 | 16 | 25.72 |
| N | 3.44 | 34.4 | 14 | 2.76 |
| S | 0.15 | 1.5 | 32 | 0.15 |

The representative substrate used in this study is based on food waste, for which average elemental composition values have been reported in the literature. According to De Clercq (2015), the wet basis elemental distribution is as follows: 47.22% carbon, 7.04% hydrogen, 41.15% oxygen, 3.86% nitrogen, and 0.49% sulfur. (De Clercq et al.,

2016)

For calculation purposes, a 1000-gram sample was assumed. The corresponding elemental masses and molar quantities are provided in Table 4.1.

Buswell's equation is expressed as follows (De Clercq et al., 2016):

$$C_cH_hO_oN_nS_s + \left(\frac{4c-h-2o+3n+2s}{4}\right)H_2O$$

$$\rightarrow \left(\frac{4c-h+2o+3n+2s}{8}\right)CO_2 + \left(\frac{4c+h-2o-3n-2s}{8}\right)CH_4 + nNH_3 + sH_2S \quad (4.1)$$

The new coefficients and calculations, based on the Buswell equation and the ratios in the resulting moles according to the elements' percentages, are calculated as shown below (De Clercq et al., 2016).

$$c = 39.35 \quad (4.2)$$

$$h = 70.4 \quad (4.3)$$

$$o = 25.72 \quad (4.4)$$

$$n = 2.76 \quad (4.5)$$

$$s = 0.15 \quad (4.6)$$

The coefficients shown above are derived directly from the generalized form of Buswell's equation, which relates the elemental composition of the substrate (in this case, food waste) to the theoretical output of key gaseous products. By substituting the calculated molar values of each element into the respective expressions, the stoichiometric yields of carbon dioxide, methane, and water are obtained as 11.04, 18.38, and 20.97 mol per mole of substrate, respectively. These values are essential for determining the mass and molar flow rates of the emitted gases and form the basis for further emission calculations (De Clercq et al., 2016).

$$\frac{4c-h-2o+3n+2s}{4} = \frac{4*39.35-70.4-2*25.72+3*2.76+2*0.15}{4} = 11.04 \quad (4.7)$$

$$\frac{4c - h + 2o + 3n + 2s}{8} =$$

$$\frac{4 * 39.35 - 70.4 + 2 * 25.72 + 3 * 2.76 + 2 * 0.15}{8} = 18.38 \quad (4.8)$$

$$\frac{4c + h - 2o - 3n - 2s}{8} =$$

$$\frac{4 * 39.35 - 70.4 - 2 * 25.72 - 3 * 2.76 - 2 * 0.15}{8} = 20.97 \quad (4.9)$$

Based on the elemental composition of the selected food waste sample and the stoichiometric results obtained from the Buswell equation, the AD reaction can be expressed as follows (De Clercq et al., 2016):

$$C_{39.35}H_{70.20}O_{25.72}N_{2.76}S_{0.15} + 11.04\ H_2O \rightarrow$$

$$18.38\ CO_2 + 20.97\ CH_4 + 2.76\ NH_3 + 0.15\ H_2S \quad (4.10)$$

This balanced reaction reflects the theoretical biogas yield from the decomposition of one mole of food waste. The methane and carbon dioxide outputs are particularly important for energy potential and emission analysis, while ammonia and hydrogen sulfide are considered due to their environmental significance.

## 4.2 Calculation Of Emission

The following subsection calculates the amount of methane required to meet the system's thermal energy demand, serving as the basis for estimating associated emission rates.

### 4.2.1 Estimation of Methane Input for Target Thermal Load

In order to operate the KC, a continuous thermal energy input of 1000 kW is assumed. This heat is provided by the combustion $CH_4$, which is the main component of the biogas produced from AD.

To calculate the amount of methane required, the HHV of methane is used. The HHV represents the total energy released when methane is completely combusted, including the latent heat of vaporization of water. According to standard thermochemical

data, the HHV of methane is taken as (Engineering ToolBox, 2001):

$$HHV_{CH_4} = 37.11\ {}^{MJ}/_{m^3} \tag{4.11}$$

Using this value, the volumetric flow rate of methane needed to meet the 1000 kW heat demand is calculated by the following equation:

$$\dot{V}_{CH_4} = \frac{\dot{Q}_{th}}{HHV_{CH_4}} = \frac{1000000\ {}^{J}/_{s}}{37.11 \times 10^6\ {}^{J}/_{m^3}} \cong 0.02695\ {}^{m^3}/_{s} \tag{4.12}$$

This value represents the minimum methane flow rate required to sustain the thermal energy input for the system under ideal combustion conditions.

### 4.2.2 Methane Volume Flow Rate Requirement

To evaluate the amount of substrate required for biogas production, the volumetric flow rate of methane must be expressed in terms of mass and moles. This enables the use of stoichiometric ratios derived from Buswell's equation (De Clercq et al., 2016).

The density of methane under standard conditions is taken as (Engineering ToolBox, 2001):

$$\rho_{CH_4} = 0.668\ {}^{kg}/_{m^3} \tag{4.13}$$

The corresponding mass flow rate of methane is then calculated as:

$$\dot{m}_{CH_4} = \dot{V}_{CH_4} \times \rho_{CH_4} \tag{4.14}$$

$$0.002695\ {}^{m^3}/_{s} \times 0.668\ {}^{kg}/_{m^3} \cong 0.018\ {}^{kg}/_{s} \tag{4.14.a}$$

To further link this to the biochemical conversion of food waste, the mass flow rate is converted into molar flow rate using the molar mass of methane (Engineering ToolBox ,2001):

$$M_{CH_4} = 16\ {}^{g}/_{mol} \tag{4.15}$$

$$\dot{n}_{CH_4} = \frac{\dot{m}_{CH_4}}{M_{CH_4}} = \frac{0.018\ {}^{kg}/_{s}}{0.016\ {}^{kg}/_{mol}} = 1.125\ {}^{mol}/_{s} \tag{4.16}$$

Once the required molar flow of methane is determined, the next step is to estimate the amount of food waste needed to generate this amount of methane through AD. This calculation is based on the theoretical methane yield obtained from the stoichiometric application of Buswell's equation, which was described in Section 1.

According to the balanced Buswell equation, the decomposition of 1 mole of food waste produces approximately 20.97 mol of $CH_4$. Using this stoichiometric ratio, the required molar input of substrate ($\dot{n}_{food\ waste}$) can be calculated as follows:

$$\dot{n}_{food\ waste} = \frac{\dot{n}_{CH_4}}{20.97} = \frac{1.125\ {}^{mol}/_{s}}{20.97} \cong 0.05365\ {}^{mol}/_{s} \tag{4.16.a}$$

An organic matter value of 0.6 was assumed for food waste in the AD process. Therefore, the required molar flow of the actual food waste input is adjusted accordingly:

$$\dot{n}_{food\ waste\ ,actual} = \frac{\dot{n}_{food\ waste}}{0.6} \tag{4.17}$$

$$\dot{n}_{food\ waste\ ,actual} = \frac{0.05365\ {}^{mol}/_{s}}{0.6} \cong 0.08942\ {}^{mol}/_{s} \tag{4.17.a}$$

This value represents the actual amount of food waste that must be processed, based on the assumed digestion efficiency, to sustain methane production at the rate required by the KC system.

### 4.2.3 Estimation of Side Gas Products from Anaerobic Digestion

In addition to methane, AD generates several other gaseous by products, such as $CO_2$, $NH_3$, and $H_2S$. These gases are formed as a result of the decomposition of the carbon, nitrogen, and sulfur components of the organic substrate, respectively.

The molar production ratios for $CO_2$, $NH_3$ and $H_2S$ were directly calculated by applying the theoretical stoichiometric yields from the Buswell equation to the actual substrate input rate, which was determined as 0.08942 mol/s. These gases were quantified based on the biodegradable fraction of the substrate, assuming 60% conversion efficiency.

However, for $CH_4$, the value presented above corresponds to the theoretical yield under conditions of complete degradation. In order to reflect realistic system performance, the actual methane yield (adjusted for degradability) is recalculated in the following section and used as the basis for subsequent energy and emission analyses.

$$1\ mol\ food\ waste\ \rightarrow\ 11.04\ mol\ H_2O \tag{4.18}$$

$$1\ mol\ food\ waste\ \rightarrow\ 18.38\ mol\ CO_2 \tag{4.19}$$

$$1\ mol\ food\ waste\ \rightarrow\ 20.97\ mol\ CH_4 \tag{4.20}$$

$$1\ mol\ food\ waste\ \rightarrow\ 2.76\ mol\ NH_3 \tag{4.21}$$

$$1\ mol\ food\ waste\ \rightarrow\ 0.15\ mol\ H_2S \tag{4.22}$$

The corresponding molar flow rates for each gas are calculated as follows:

$$\dot{n}_{H_2O} = 0.08942\ \times 11.04 = 0.9872\ {}^{mol}/_{S}\ for\ H_2O \tag{4.23}$$

$$\dot{n}_{CO_2} = 0.08942\ \times 18.38 = 1.643\ {}^{mol}/_{S}\ for\ CO_2 \tag{4.24}$$

$$\dot{n}_{CH_4,actual} = 0.08942\ \times 20.97 = 1.875\ {}^{mol}/_{S}\ for\ CH_4 \tag{4.25}$$

$$\dot{n}_{NH_3} = 0.08942\ \times 2.76 = 0.2468\ {}^{mol}/_{S}\ for\ NH_3 \tag{4.26}$$

$$\dot{n}_{H_2S} = 0.08942\ \times 0.15 = 0.01341\ {}^{mol}/_{S}\ \ for\ H_2S \tag{4.27}$$

These molar flow rates represent the theoretical emission rates of each gas under steady state operation of the AD process, assuming complete conversion efficiency based on the elemental composition of the food waste input.

To evaluate the environmental impact of the gases produced during AD, the molar flow rates calculated in the previous section must be converted into mass flow rates (kg/s). This allows for direct comparison with regulatory thresholds and emission inventories.

The conversion is performed using the molar masses of each gas (Engineering ToolBox, 2001):

$$M_{H_2O} = 18\ {}^{g}/_{mol} \tag{4.28}$$

$$M_{CO_2} = 44\ {}^{g}/_{mol} \tag{4.29}$$

$$M_{CH_4} = 16\ {}^{g}/_{mol} \tag{4.30}$$

$$M_{NH_3} = 17\ {}^{g}/_{mol} \tag{4.31}$$

$$M_{H_2S} = 34\ {}^{g}/_{mol} \tag{4.32}$$

Accordingly, the mass flow rates are:

$$\dot{m}_x = \dot{n}_x \times M_x \tag{4.33}$$

$$\dot{m}_{H_2O} = 0.018\ {}^{kg}/_{mol} \times 0.9872\ {}^{mol}/_{s} = 0.01777\ {}^{kg}/_{s}\ for\ H_2O \tag{4.33.a}$$

$$\dot{m}_{CO_2} = 0.044\ {}^{kg}/_{mol} \times 1.643\ {}^{mol}/_{s} = 0.07231\ {}^{kg}/_{s}\ for\ CO_2 \tag{4.33.b}$$

$$\dot{m}_{CH_4,\ actual} = 0.016\ {}^{kg}/_{mol} \times\ 1.875\ {}^{mol}/_{s} = 0.03\ {}^{kg}/_{s}\ for\ CH_4 \tag{4.33.c}$$

$$\dot{m}_{NH_3} = 0.017\ {}^{kg}/_{mol} \times\ 0.2468\ {}^{mol}/_{s} = 0.004195\ {}^{kg}/_{s}\ for\ NH_3 \tag{4.33.d}$$

$$\dot{m}_{H_2S} = 0.034\ {}^{kg}/_{mol} \times 0.01341\ {}^{mol}/_{s} = 0.0004559\ {}^{kg}/_{s}\ \ for\ H_2S \tag{4.33.e}$$

While carbon dioxide is a well-recognized GHG, $NH_3$ and $H_2S$ are not classified GHG under current IPCC frameworks. Nevertheless, both gases have significant environmental implications. Ammonia contributes to eutrophication and acidification when released into natural ecosystems, while hydrogen sulfide poses serious health risks due to its toxicity, even at low concentrations, particularly in confined or poorly ventilated environments.

Therefore, although these emissions are not regulated as GHGs, these emissions were included in the present analysis to provide a more comprehensive assessment of the system's overall environmental performance.

Although the primary analysis in this study focuses on calculations based on molar quantity and mass, the volumetric flow rates of individual gaseous products can also be derived using standard gas densities under standard conditions.

For instance, using the standard gas densities at 25°C and 1 atm (Engineering ToolBox, 201):

$$\rho_{H_2O} = 997.05\ {}^{kg}/_{m^3} \tag{4.34}$$

$$\rho_{CO_2} = 1.842\ {}^{kg}/_{m^3} \tag{4.35}$$

$$\rho_{CH_4} = 0.668\ {}^{kg}/_{m^3} \tag{4.36}$$

$$\rho_{NH_3} = 0.771\ {}^{kg}/_{m^3} \tag{4.37}$$

$$\rho_{H_2S} = 1.434\ {}^{kg}/_{m^3} \tag{4.38}$$

The corresponding volumetric flow rates can be calculated as follows:

$$\dot{V}_x = \frac{\dot{m}_x}{\rho_x} \tag{4.39}$$

$$\dot{V}_{H_2O} = \frac{0.01777\ {}^{kg}/_{s}}{997.05\ {}^{kg}/_{m^3}} = 0.00001782\ {}^{m^3}/_{s}\ for\ CO_2 \tag{4.39.a}$$

$$\dot{V}_{CO_2} = \frac{0.07231\ {}^{kg}/_{s}}{1.842\ {}^{kg}/_{m^3}} = 0.03926\ {}^{m^3}/_{s}\ for\ CO_2 \tag{4.39.b}$$

$$\dot{V}_{CH_4,\ actual} = \frac{0.03\ {}^{kg}/_{s}}{0.668\ {}^{kg}/_{m^3}} = 0.4491\ {}^{m^3}/_{s}\ for\ CH_4 \tag{4.39.c}$$

$$\dot{V}_{NH_3} = \frac{0.004195\ {}^{kg}/_{s}}{0.717\ {}^{kg}/_{m^3}} = 0.005851\ {}^{m^3}/_{s}\ for\ NH_3 \tag{4.39.d}$$

$$\dot{V}_{H_2S} = \frac{0.0004559\ {}^{kg}/_{s}}{1.434\ {}^{kg}/_{m^3}} = 0.0003179\ {}^{m^3}/_{s}\ for\ H_2S \tag{4.39.e}$$

These values were not used in the emission inventory calculations but are documented here for completeness and to support any future process scale modeling.

The final results of all calculations presented in the previous sections are summarized in Table 4.2 below. It includes the volumetric, molar, and mass flow rates of the main gaseous products derived from the AD process. These values offer a comprehensive overview of the gas composition that offer the KC system.

**Table 4.2:** Summary of calculated gas flow rates from AD process.

| | Mole Flow Rate (mol/s) | Mass Flow Rate (kg/s) | Density (kg/m3) | Volume Flow Rate (m3/s) |
|---|---|---|---|---|
| $H_2O$ | 0.9872 | 0.01777 | 997.05 | 0.00001782 |
| $CO_2$ | 1.643 | 0.07231 | 1.842 | 0.03926 |
| $NH_3$ | 0.2468 | 0.004195 | 0.717 | 0.005851 |
| $CH_4$ | 1.875 | 0.03 | 0.668 | 0.4491 |
| $H_2S$ | 0.01341 | 0.0004559 | 1.434 | 0.0003179 |

### 4.2.4 Integration of Methane Combustion with the Kalina Cycle System

The methane used in this study is not supplied from an external fossil source but is rather derived from the AD of food waste, as outlined in the previous sections. After its production and purification, the methane of biological origin is directed to controlled combustion to provide the thermal energy input required by the KC.

Instead of releasing this high-impact GHG into the atmosphere, it is combusted with a thermal efficiency of 98% (Intergovernmental Panel on Climate Change [IPCC],2006) enabling maximum energy recovery and minimizing unburned emissions. The heat generated in this process is transferred to the working fluid of the KC through the primary heat exchanger, initiating the thermodynamic cycle. In this framework, methane does not act as a conventional fuel but rather as a medium that enables the conversion of waste into usable energy within a closed loop system.

This configuration offers dual benefits: it enables the valorization of food waste by converting it into useful thermal energy, and it prevents the uncontrolled release of

methane, which has a global warming potential 25 times greater than $CO_2$. The efficiency of methane combustion and its integration into the KC system forms the basis for the emission evaluations conducted in subsequent sections.

The combustion reaction of methane:

$$CH_4 + 2O_2 = CO_2 + 2H_2O \tag{4.40}$$

### 4.2.5 Emission Estimation Methodology

The general equation for emission estimation is given as (IPCC,2006):

$$\dot{m}_{gas} = Emission\ Factor \times LHV \tag{4.41}$$

The emission factors used in this study for the calculation of combustion related GHG are presented in Table 4.3. Each factor is expressed in kilograms of emitted gas per terajoule of thermal energy input (kg/TJ**)**. The three gases considered $CO_2$, $CH_4$, and $N_2O$ represent the major GHG species associated with methane combustion.

**Table 4.3:** Default emission factors for stationary combustion in the energy industries (kg of GHG per TJ on a net calorific basis) (IPCC ,2006)

| | $CO_2$ kg/TJ | $N_2O$ kg/TJ | $CH_4$ kg/TJ |
|---|---|---|---|
| Emission Factors | 56100 | 0.1 | 1 |

The emission factor for $CO_2$ reflects the complete oxidation of carbon content within methane and has the highest magnitude due to the stoichiometric yield of carbon dioxide. The $CH_4$ and $N_2O$ factors represent minor fractions of incomplete combustion and trace formation of nitrous oxide, respectively. These standardized values allow for consistent and internationally comparable estimations when data specific to each country or based on direct measurements are unavailable.

In this study, the emission factors used for calculating the emissions from methane combustion are listed in Table 4.4. (IPCC, 2006). These emission factors were used together with the calculated amount of combusted methane, which was determined based on LHV and mass flow rate. The emissions of each gas were calculated by multiplying

the relevant emission factor with the corresponding mass flow rate of methane.

LHV of methane is 50.49 MJ/kg (Engineering ToolBox, 2001).

$$\dot{m}_{CH_4,\ burned} = 0.0294\ {}^{kg}/_{s} \times 50.49\ {}^{MJ}/_{kg} \times 1\ {}^{kg}/_{TJ} \times 10^{-6}\ {}^{TJ}/_{MJ}$$

$$= 1.4844 \times 10^{-6}\ {}^{kg}/_{s} \quad (4.42)$$

$$\dot{m}_{CH_4,\ unburned} = 0.0006\ {}^{kg}/_{s} \times 50.49\ {}^{MJ}/_{kg} \times 1\ {}^{kg}/_{TJ} \times 10^{-6}\ {}^{TJ}/_{MJ}$$

$$= 3.029 \times 10^{-8}\ {}^{kg}/_{s} \quad (4.43)$$

$$\dot{m}_{CO_2} = 1.4844 \times 10^{-6}\ {}^{TJ}/_{s} \times 56100\ {}^{kg}/_{TJ}$$

$$= 0.08327\ {}^{kg}/_{s}\ for\ CO_2 \quad (4.44)$$

$$\dot{m}_{N_2O} = 1.4844 \times 10^{-6}\ {}^{TJ}/_{s} \times 0.1\ {}^{kg}/_{TJ}$$

$$= 1.4844 \times 10^{-7}\ {}^{kg}/_{s}\ for\ N_2O \quad (4.45)$$

**Table 4.4:** Calculated GHG emission rates from methane combustion (kg/s).

| | $CO_2$ (kg/s) | $N_2O$ (kg/s) | $CH_4$ (unburned kg/s) |
|---|---|---|---|
| Emission | 0.08327 | $1.4844 \times 10^{-7}$ | $3.029 \times 10^{-8}$ |

In this study, carbon dioxide emissions arise from two distinct sources. The first component is generated during the AD of food waste, as based on the stoichiometric predictions of the Buswell equation (De Clercq, 2016). This represents the biogenic $CO_2$ released as a direct byproduct of the degradation process. The second component is results from the subsequent combustion of the methane produced in the digestion stage.

To obtain a complete representation of the carbon dioxide output from the system, both contributions are considered. The total $CO_2$ emission is therefore expressed as the sum of the digestion related and combustion related values, providing a comprehensive estimate of the system's carbon release profile.

$$\dot{m}_{CO_2,\ total} = 0.07231\ {}^{kg}/_{s} + 0.08327\ {}^{kg}/_{s} = 0.1556\ {}^{kg}/_{s} \quad (4.46)$$

$$\dot{m}_{N_2O} = 1.4844 \times 10^{-7}\ {}^{kg}/_{s} \quad (4.47)$$

$$\dot{m}_{CH_4} = 3.029 \times 10^{-8}\ {}^{kg}/_{s} \quad (4.48)$$

The combustion of methane produces $CO_2$ and $N_2O$. In this study, it is assumed that 98% of the produced $CH_4$ is combusted, while the remaining 2% is directly released into the atmosphere as unburned methane. Therefore, $CO_2$ and $N_2O$ emissions are calculated based on the combusted fraction of $CH_4$. The remaining 2% is released as unburned $CH_4$, contributing directly to GHG emissions.

# 5. COST ANALYSIS FOR EMISSION GASES

In this section, a dual-focused economic analysis was conducted to evaluate the mitigation costs of the major greenhouse gases emitted from the system: $CO_2$ and $N_2O$. For the $CO_2$ component, a post-combustion calcium looping (CaL) method was adopted as the capture strategy. This process involves a cyclic reaction scheme in which $CO_2$ from the flue gas reacts with CaO to form $CaCO_3$, which is then regenerated in a calciner. The methodology followed includes calculating the annual mass of $CO_2$ emitted, determining the amount captured based on an assumed capture efficiency, and then estimating the total CaO demand using stoichiometric molar ratios. Additionally, the share of fresh CaO input, electricity requirement per unit $CO_2$ captured, and annualized CAPEX and OPEX were taken into account. All cost components were then aggregated to determine the overall economic impact of the $CO_2$ capture subsystem.

For $N_2O$, which is present in lower quantities but has a significantly higher global warming potential, a catalytic decomposition approach was considered. Specifically, the analysis focused on Co-ZSM-5-based catalysts, which have demonstrated strong performance in decomposing $N_2O$ under industrially relevant conditions. The decomposition process was modeled as a continuous operation with assumed complete conversion, and the cost analysis included estimated catalyst expenses and the energy input required to maintain the operational temperature. As with the $CO_2$ subsystem, the methodology involved calculating the annual mass flow of $N_2O$, estimating

decomposition costs per unit mass, and projecting total annual expenditure based on realistic system operation assumptions.

By following these structured approaches for both gases, the aim is to provide a comparative understanding of their mitigation economics and to guide the integration of emission control measures into the broader thermodynamic cycle.

## 5.1 Cost Analysis of the $CO_2$ Capture System Using CaO

In this study, an integrated approach is proposed in which the $CO_2$ capture subsystem is embedded within a KC biomass power plant. The selected capture method is based on the calcium looping (CaL) concept. In this method, $CO_2$ from flue gases reacts with calcium oxide in a carbonator to form $CaCO_3$. This compound is then regenerated in a separate reactor called a calciner, where $CaCO_3$ decomposes back into CaO and a concentrated $CO_2$ stream. This closed-loop process enables the continuous use of solid sorbents (Abanades et al., 2002) During the carbonation step, CaO reacts with $CO_2$ to form $CaCO_3$, enabling the separation of $CO_2$ from the exhaust stream. The sorbent is then regenerated in a calciner via thermal decomposition, allowing the CaO to be reused in a continuous cycle.

The process includes two distinct stages known as carbonation and calcination. In the carbonation reactor, $CO_2$-rich flue gas comes into contact with CaO at a temperature of approximately 650 to 700°C. During this exothermic reaction, $CaCO_3$ is formed (Abanades et al., 2002). This process, commonly referred to as post-combustion calcium looping, is governed by the following exothermic reaction:

$$CaO(s) + CO_2(g) \rightarrow CaCO_3(s) \qquad \Delta H = -177\frac{kJ}{mol} \tag{5.1}$$

The solid product is then transferred to the calcination reactor. In this second stage, the temperature is increased above 900°C under an oxy-fuel atmosphere (Abanades et al., 2002), which allows decomposition of $CaCO_3$ into CaO and $CO_2$ through an endothermic reaction:

$$CaCO_3(s) \rightarrow CaO(s) + CO_2(g) \qquad \Delta H = 177\frac{kJ}{mol} \tag{5.2}$$

The $CO_2$ released in the calciner is highly concentrated and suitable for compression and storage. The regenerated CaO is reintroduced into the carbonation reactor, forming a closed-loop system. However, with each reaction cycle, the physical properties of the CaO particles begin to degrade. Surface sintering and pore blockage reduce sorbent reactivity. This degradation leads to a gradual reduction in the $CO_2$ capture capacity of the material (Martínez et al., 2013).

To maintain stable system performance, a portion of the sorbent must be purged from the loop. Fresh CaO is then added in its place. The ratio of fresh CaO to the total circulating sorbent directly affects both the operating cost and the capture efficiency. A well-optimized system maintains a fresh CaO flow rate that ensures adequate reactivity while minimizing resource consumption (Abanades et al., 2004).

The calcium looping system operates at high temperatures and offers the potential to recover heat from both the carbonator and calciner. The thermal energy released during these processes can be integrated into a secondary steam cycle to generate electricity. This co-generation of power offsets a portion of the capture-related energy cost (Romeo et al., 2008)

For realistic industrial applications, the capture efficiency typically falls in the range of 75% to 90%. This range represents a trade-off between the cost of maintaining high reactivity and the diminishing returns associated with extreme purification targets. Literature studies often assume an average capture efficiency of 80% when evaluating the cost-effectiveness of calcium looping (Grasa and Abanades, 2006).

### 5.1.1 System Parameters and Economic Inputs for CO2 Capture

This section presents a revised cost evaluation of a post-combustion $CO_2$ capture system based on the calcium looping (CaL) process. All calculations were updated using current prices and the stoichiometric reaction basis, while assuming a capture efficiency of $CO_2$ ($\eta_{cap}$) as 80%. The following parameters were adopted:

**Table 5.1:** Key parameters used for the economic evaluation of $CO_2$ capture using CaO-based looping.

| Parameter | Symbol/ Description | Value | Unit |
|---|---|---|---|
| Outlet $CO_2$ mass flow rate | $\dot{m}_{CO_2}$ | 0.1556 | kg/s |
| $CO_2$ capture efficiency | $\eta_{cap}$ | 80 | % |
| Operating time | Annual operation | 8760 | Hours/year |
| Electricity price | - | 0.1 | €/kWh |
| Fresh CaO cost | - | 100 | €/ton |
| Electricity consumption for $CO_2$ capture | Per unit $CO_2$ captured | 41.67 | Wh/kg $CO_2$ |
| Fresh CaO make-up ratio | $x_p$ | 0.4 | - |
| Molar ratio (CaO / $CO_2$) | Stoichiometric basis | 1 | mol/mol |
| Molar mass of $CO_2$ | $M_{CO_2}$ | 44.01 | g/mol |
| Molar mass of CaO | $M_{CaO}$ | 56.08 | g/mol |

### 5.1.2 Economic Evaluation of $CO_2$ Capture System

For $CO_2$ capturing process, first, the annual mass of $CO_2$ emitted is calculated from the outlet flow:

$$\dot{m}_{CO_2} = 0.1556 \frac{kg}{s} \tag{5.3}$$

$$Total\ CO_2\ emitted\ per\ year\ (F_{CO_2}) = \dot{m}_{CO_2}.\frac{3600s}{h}.\frac{8760h}{year} = \frac{4{,}904{,}256kg}{year}$$

$$= 4904.26 \frac{ton}{year} \tag{5.4}$$

Then, using a capture efficiency of 80%:

$$Captured\ CO_2 = \eta_{cap}.F_{CO_2} = 0.80\ x\ 4904.26 = 3923.41 \frac{ton}{year} \tag{5.5}$$

For CaO consumption, the stoichiometric molar mass ratio is:

$$\frac{M_{CaO}}{M_{CO_2}} = \frac{56.08}{44.01} = 1.2745 \tag{5.6}$$

Thus, the total annual CaO demand becomes:

$$Total\ CaO\ used = Captured\ CO_2 \times \frac{M_{CaO}}{M_{CO_2}} \tag{5.7}$$

$$Total\ CaO\ used = 3923.41 \times 1.2745 = 5000.86 \frac{ton}{year} \tag{5.8}$$

Assuming 40% of the total CaO must be fresh:

$$Fresh\ CaO = x\square \times Total\ CaO\ used \tag{5.9}$$

$$Fresh\ CaO = 0.4 \times 5000.86 = 2000.34 \frac{ton}{year} \tag{5.10}$$

Calculating cost of fresh CaO:

$$Cost\ of\ fresh\ CaO = Fresh\ CaO \times Cost\ of\ CaO \tag{5.11}$$

$$Cost\ of\ fresh\ CaO = 2000.34 \times 100 = \frac{200{,}034€}{year} \tag{5.12}$$

$$Cost\ of\ per\ ton\ CO_2\ = \frac{Cost\ of\ fresh\ CaO}{Captured\ CO_2} \tag{5.13}$$

$$Cost\ of\ per\ ton\ CO_2\ = \frac{200{,}034}{3923.41} = \frac{50.98€}{ton\ CO_2} \tag{5.14}$$

In order to determine the electricity consumption per unit of captured $CO_2$, the specific energy demand is taken as 0.15 MJ per kg of $CO_2$, as reported in previous studies (Romeo et al., 2008). This value is then converted to watt-hours using the standard energy conversion factor:

$$0.15\frac{MJ}{kgCO_2}x\frac{277.78\,Wh}{MJ} = 41.67\frac{Wh}{kgCO_2} = \frac{0.04167kWh}{kgCO_2} \quad (5.15)$$

This value represents the amount of electricity required to capture 1 kg of $CO_2$ in the system.

Annual electricity consumption for captured $CO_2$

$$Total\ electricity\ use = 3923.41 \times 1000 \times 0.04167 = \frac{163{,}578kWh}{year} \quad (5.16)$$

$$Total\ Electricity\ cost = 163{,}578 \times 0.10 = \frac{16{,}358€}{year} \quad (5.17)$$

$$Electricity\ cost\ per\ ton\ CO_2 = \frac{16{,}358}{3923.41} = 4.17€/ton\ CO_2 \quad (5.18)$$

Operation and maintenance (O&M), capital expenditures (CAPEX) and operational expenditures (OPEX) are assumed as :

**Table 5.2:** Breakdown of cost components associated with $CO_2$ capture per ton of $CO_2$ removed.

| **Cost Component** | **Cost per ton $CO_2$ (€/ton $CO_2$)** |
|---|---|
| CAPEX | 40 |
| OPEX | 14 |
| O&M | 20 |

$$CAPEX = 40 \times\ 3923.41 = 156{,}936.4€/year \quad (5.18)$$

$$OPEX = 14 \times 3923.41 = 54{,}927.74€/year \quad (5.19)$$

$$O\&M = 20\ \times\ 3923.41 =\ 78{,}468.2€/year \quad (5.20)$$

Summing all annual cost components:

$$Total\ Cost = 200{,}034 + 16{,}358 + 156{,}936.4 + 54{,}927.74 + 78{,}468.2 = 506{,}724.34€/year \quad (5.21)$$

$$Cost\ cost\ per\ ton\ CO_2 = \frac{506{,}724.34}{3923.41} = 129.15€/ton\ CO_2 \quad (5.22)$$

To find this value (Eq.5.22), a detailed techno-economic analysis was performed to evaluate the annual cost of capturing $CO_2$ via a post-combustion CaL system. The calculations were based on a $CO_2$ mass flow rate of 0.1556 kg/s and an assumed capture efficiency of 80%, resulting in an annual $CO_2$ removal of approximately 3,923.41 tons. To achieve this, a 1:1 CaO to $CO_2$ molar ratio was adopted, with 40% of the total CaO input considered as fresh make-up material, in line with literature assumptions. The cost of fresh CaO was taken as 100 €/ton, and the electricity consumption was assumed as 0.15 MJ/kg $CO_2$ based on energy penalty data from similar capture systems, with a contemporary electricity price of 0.10 €/kWh. CAPEX and OPEX were included at rates of 40 €/ton $CO_2$ and 14 €/ton $CO_2$, respectively, while operation and maintenance (O&M) costs were estimated as 20 €/ton $CO_2$. These values were selected to reflect current industrial conditions as closely as possible. Summing all cost components, the total annual expenditure for the capture system was calculated as approximately 506,724.34 €/year, which corresponds to a specific cost of 129.15 €/ton $CO_2$ captured.

## 5.2 Cost Analysis of the Catalytic Decomposition of $N_2O$

$N_2O$ is a highly potent greenhouse gas, with a global warming potential nearly 300 times greater than that of $CO_2$ on a per-mass basis. (IPCC,2006) It is released as a byproduct during combustion processes, including the oxidation of nitrogen-containing fuels and residual ammonia in power generation systems. Due to its longevity in the atmosphere and its significant environmental impact, the reduction of $N_2O$ emissions has become a critical challenge in emission control strategies.

One of the most effective and technically mature methods for mitigating $N_2O$ emissions is catalytic decomposition. This process offers notable advantages because it does not require external reducing agents, additives, or multiple reactants, allowing for a cleaner and more stable operation under suitable conditions. The thermal decomposition

of $N_2O$ occurs above 850°C, producing $N_2$ and $O_2$ as per the following reaction (Seçkin et al., 2013):

$$N_2O \rightarrow N_2 + {}^1/_2\, O_2 \qquad \Delta H = -82\frac{kJ}{mol} \tag{5.23}$$

This reaction becomes thermodynamically favorable at temperatures above 600°C, and complete conversion is typically achieved when the temperature exceeds 800°C under pure thermal decomposition conditions. (Galle et al., 2001). However, such high-temperature operation demands significant energy input, which can increase the overall cost of the abatement process.

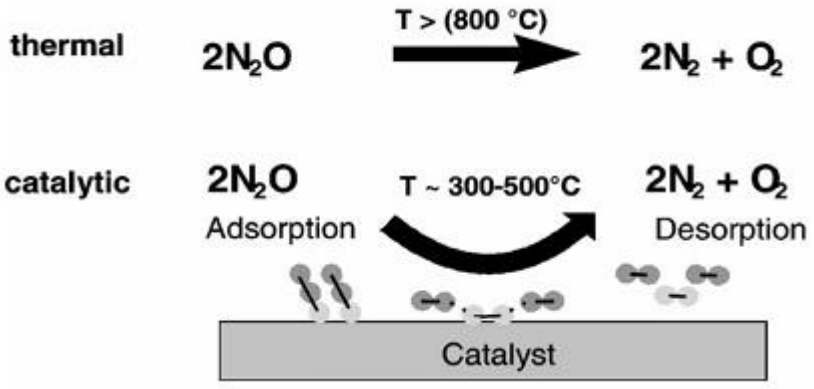


**Figure 5.1:** $N_2O$ decomposition paths.

To reduce the temperature requirement while maintaining high decomposition efficiency, metal-exchanged zeolite catalysts have been developed. Among them, Co-ZSM-5 has proven to be particularly effective. This cobalt-based catalyst enables the decomposition of $N_2O$ within a reduced temperature range, typically between 300°C and 500°C (Fig 23), which makes it suitable for energy-efficient applications. (Galle et al., 2001)

Co-ZSM-5 promotes the dissociation of the N–O bond by forming reactive cobalt-oxygen complexes on the zeolite framework. The catalytic surface facilitates the adsorption of $N_2O$ molecules and promotes their breakdown into $N_2$ and $O_2$, enhancing the overall reaction kinetics. In addition, the catalyst exhibits high thermal stability and maintains its activity in the presence of excess oxygen and water vapor, making it applicable to flue gas treatment systems where these species are abundant. (Cruz et al.,1998)

This catalytic behavior allows Co-ZSM-5 to be used effectively in post-combustion setups or integrated into waste heat recovery units, where moderate temperatures are already available. Its combination of activity, selectivity, and resilience under industrial conditions makes it a strong candidate for practical $N_2O$ emission control.

### 5.2.1 Economic Evaluation of $N_2O$ Decomposition Using Co-ZSM-5 Catalyst

In this study, a catalytic decomposition method is selected to mitigate the nitrous oxide ($N_2O$) emissions from the Kalina Cycle biomass power plant. Specifically, cobalt-exchanged zeolite (Co-ZSM-5) is chosen due to its strong thermal stability, resistance to water vapor, and excellent decomposition efficiency at moderate temperatures between 400–600°C. The assumed decomposition efficiency is taken as 100% due to the continuous operation under optimized conditions.

The literature used in this study (da Cruz et al., 1998) provides detailed catalytic performance data for Co-ZSM-5 catalysts with known cobalt content (e.g., 3.76 wt% Co), but does not directly specify the required mass of catalyst per mole of $N_2O$ decomposed. Additionally, no cost data is presented in the study. Therefore, an indirect estimation approach was applied by assuming a basis for catalytic activity derived from the experimental testing conditions provided in the article.

The experimental section of the referenced study indicates that 100 mg of Co-ZSM-5 catalyst was used in each test, where the sample had a cobalt content of 3.76 wt%. It is also reported that under steady-state conditions at optimal temperatures (above 500 °C), complete $N_2O$ conversion was achieved in a continuous flow reactor. Based on this, it was assumed that 100 mg of Co-ZSM-5 is sufficient to fully decompose 1 mol of $N_2O$ under ideal laboratory conditions. Using this assumed stoichiometric relationship, the amount of catalyst required to treat any specified mass of $N_2O$ can be calculated.

Since Co-ZSM-5 is not commercially available in pre-loaded form, the catalyst must be synthesized in the laboratory using a parent ZSM-5 zeolite and cobalt precursor. The synthesis procedure involves ion exchange using cobalt nitrate ($Co(NO_3)_2 \cdot 6H_2O$), followed by drying, pH adjustment using diluted ammonia solution, and calcination. Based on the unit prices of laboratory chemicals and utilities, the estimated cost of

producing Co-ZSM-5 at laboratory scale is approximately €7.1 per gram. This cost includes the zeolite (ZSM-5) base material, the cobalt precursor, pH-adjusting reagents, and the energy input required for drying and calcination processes.

The input value for $N_2O$ emission is taken from the mass flow of the system:

$$\dot{m}_{N_2O} = 1.4844\ x\ 10^{-7}\frac{kg}{s} \tag{5.24}$$

Assuming continuous yearly operation:

$$\dot{m}_{N_2O} = 1.4844\ x\ 10^{-7} x\ 3600\ x\ 24\ x\ 365 = 4.683\frac{kg}{year} \tag{5.25}$$

With the molar mass of $N_2O$ being 44.01 g/mol, this corresponds to:

$$\frac{4.683\ kg}{44.01\frac{g}{mol}} = 106.4\frac{mol}{year} \tag{5.26}$$

Assuming 100 mg of catalyst is required per mole of $N_2O$:

$$106.4\ mol \times \frac{0.1\ g}{mol} = 10.64\ g\ Co - ZSM - \frac{5}{year} \tag{5.27}$$

The total annual cost of the catalyst is then:

$$10.64\ g \times \frac{€7.1}{g} = €75.5\ per\ year \tag{5.28}$$

In summary, the decomposition of 106.4 mol (4.683 kg) of $N_2O$ annually would require approximately 10.64 grams of Co-ZSM-5 catalyst. To produce this quantity of catalyst in the laboratory, about 10.64 g of ZSM-5 zeolite and 0.4 g of cobalt (from $Co(NO_3)_2 \cdot 6H_2O$) are required, along with small amounts of ammonia solution and heat energy for calcination. The total production cost is approximately €75.5 per year under laboratory-scale assumptions.

# 6. RESULTS AND DISCUSSION

This chapter presents the main outcomes of the thermodynamic and environmental analysis of KC system operating with biomethane derived from AD. The effects of working fluid mass flow rate and turbine inlet temperature were examined with respect to energy performance and emission-based evaluation. The results are interpreted in line with the objectives of the study and compared with relevant literature.

## 6.1 Effect of Operating Parameters on Energy Performance

An increase in the working fluid mass flow rate results in higher net power output due to enhanced heat absorption and vapor generation. As the mass flow increases, more fluid passes through the heat exchanger, which allows more energy to be carried into the turbine. Thermal efficiency also improves, although more gradually, since additional input energy does not fully translate into output beyond a certain point. These results are presented in Figure 11.

Raising the turbine inlet temperature also improves both energy indicators. Higher temperature increases the enthalpy of the fluid entering the turbine, which allows more mechanical work to be extracted. However, the gains become smaller at high temperature values, as the working fluid begins to approach its thermodynamic limits. Figure 17 demonstrates this behavior, which agrees with earlier findings by Wang et al. (2019) and Seçkin (2020).

## 6.2 Energy Performance per Unit Emission

To understand the environmental effectiveness of the system, energy output and thermal efficiency were recalculated based on the mass of each emitted gas. This approach makes it possible to evaluate how efficiently the system performs relative to its environmental load.

### 6.2.1 Effect of Total Mass Flow Rate

This section examines how changes in the working fluid mass flow rate affect the performance of the KC. The analysis is based on net power output and thermal efficiency

across different flow conditions.

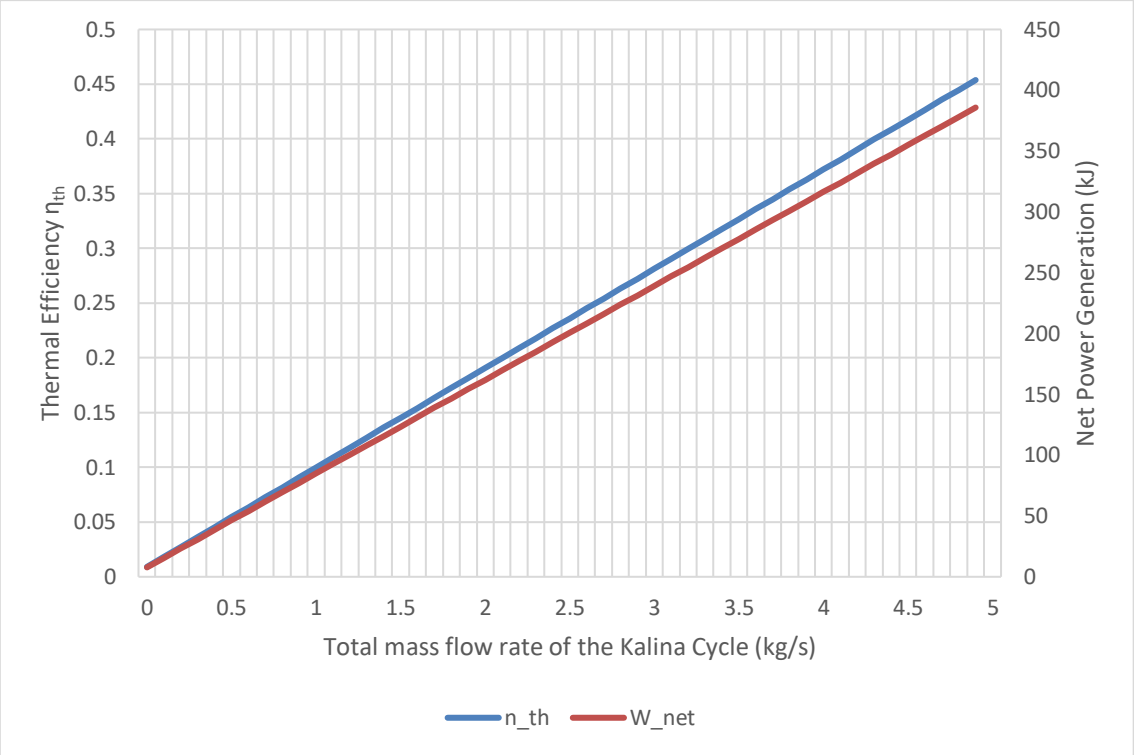


**Figure 6.1:** Variation of net power generation and thermal efficiency with respect to total mass flow rate in the Kalina cycle.

Figure 6.1 presents the variation of the KC's net power generation and thermal efficiency as functions of the total mass flow rate of the working fluid. Both performance indicators increase almost linearly as the mass flow rate rises, clearly showing that higher fluid flow leads to improved system performance. As the flow rate increases, more thermal energy is transferred to the working fluid, resulting in a higher degree of vaporization and, consequently, greater turbine work output. This proportional growth in net power stems from enhanced energy exchange within each component of the cycle due to the increased working fluid mass.

In contrast, the thermal efficiency curve, although also increasing, does so at a slightly reduced rate, indicating diminishing returns in energy conversion effectiveness as the energy input rises. This divergence reflects the fundamental difference between the two indicators: while net power quantifies absolute mechanical output, thermal efficiency expresses the ratio of useful output to energy input. The trends observed confirm that, within the tested operational range, the KC exhibits stable and scalable behaviour, with

both output metrics improving without signs of saturation or thermodynamic limitations.

Figures 6.2 through 6.6, each corresponding to a specific emission gas, show similar trends, where both net power output and thermal efficiency continue to rise steadily with increasing mass flow rate. In contrast, these graphs focus on performance per unit of emission rather than absolute values.

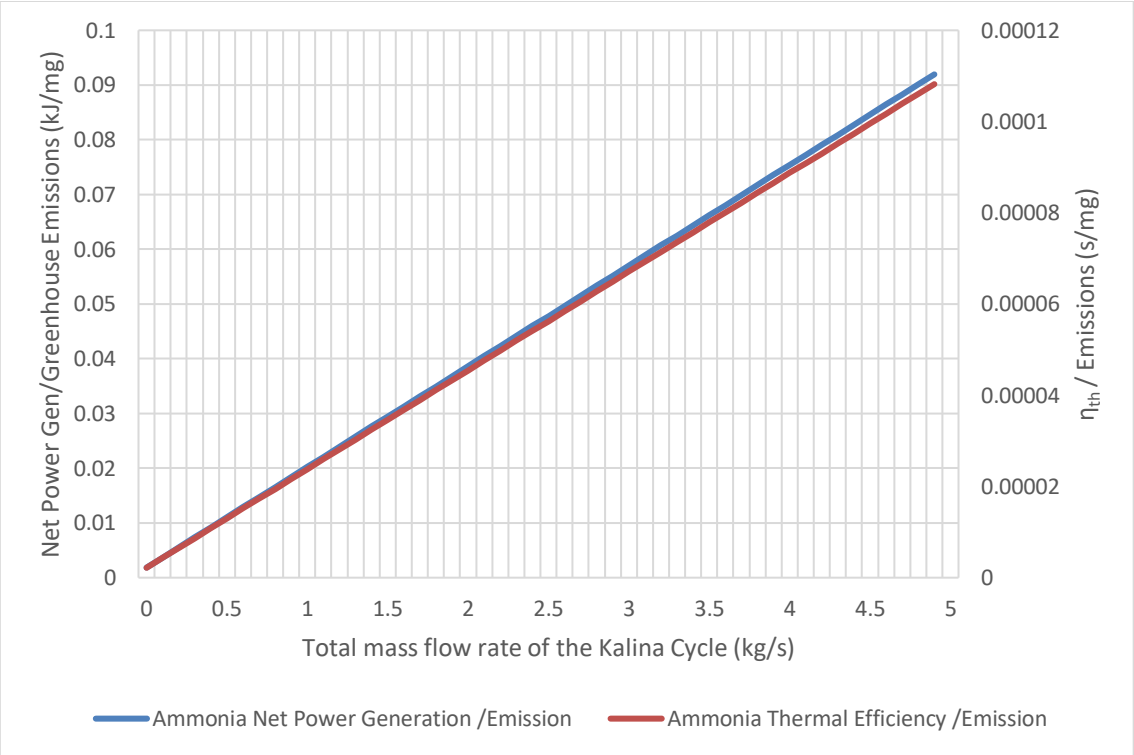


**Figure 6.2:** Variation of net power generation to $NH_3$ emission and thermal efficiency to $NH_3$ emission ratios with respect to total working fluid mass flow rate in the Kalina cycle.

Figure 6.2 shows that as the mass flow rate of the working fluid increases, both net power generation and thermal efficiency per unit of $NH_3$ emission also rise. However, this increase is relatively limited when compared to the trends observed for other emission gases. Because $NH_3$ is released as a byproduct of the AD of food waste, not from combustion, variations in mass flow rate do not directly affect its emission level. As a result, although the overall system performance improves with increased flow, the performance indicators based on ammonia emissions show less improvement than those associated with other gases.

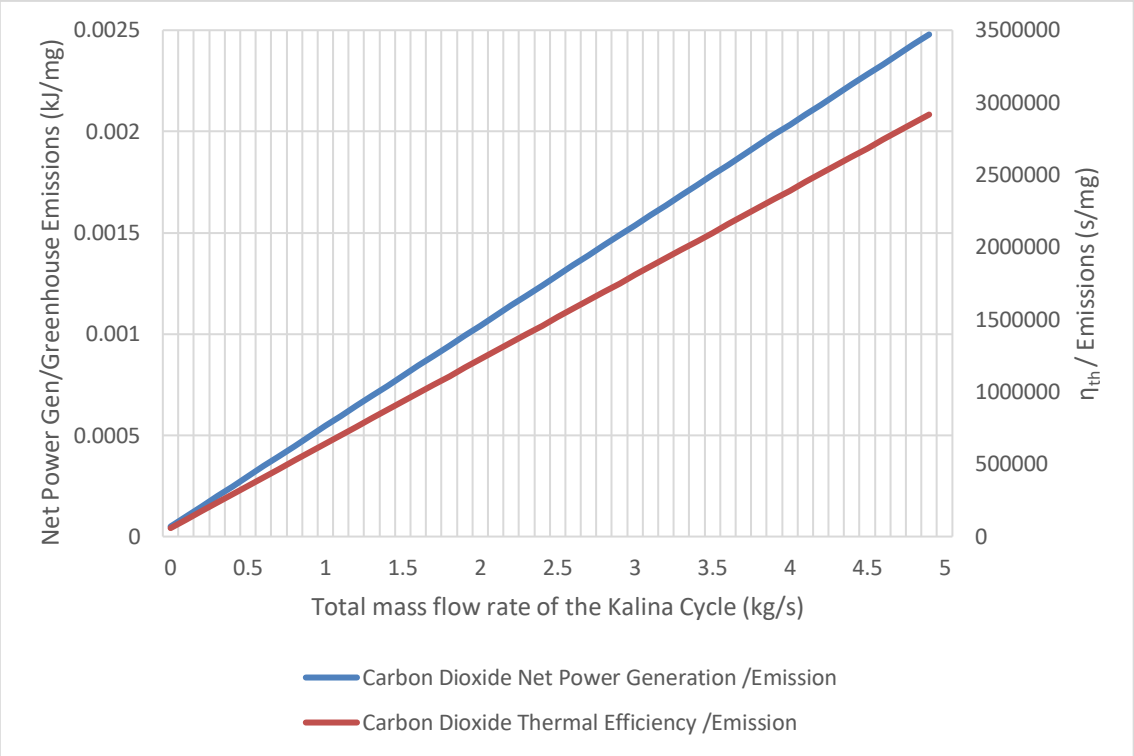


**Figure 6.3:** Variation of net power generation to $CO_2$ emission and thermal efficiency to $CO_2$ emission ratios with respect to total working fluid mass flow rate in the Kalina cycle.

Figure 6.3 shows that both net power output and thermal efficiency per unit of $CO_2$ emission increase as the mass flow rate rises. However, the rate of increase in these values is lower than what is observed for other emission gases. This is due to the fact that $CO_2$ is emitted in large quantities, both from methane combustion and from the AD of food waste. Because the values are calculated relative to emission amounts, the high volume of $CO_2$ reduces these indicators, making the results appear modest even when system performance improves.

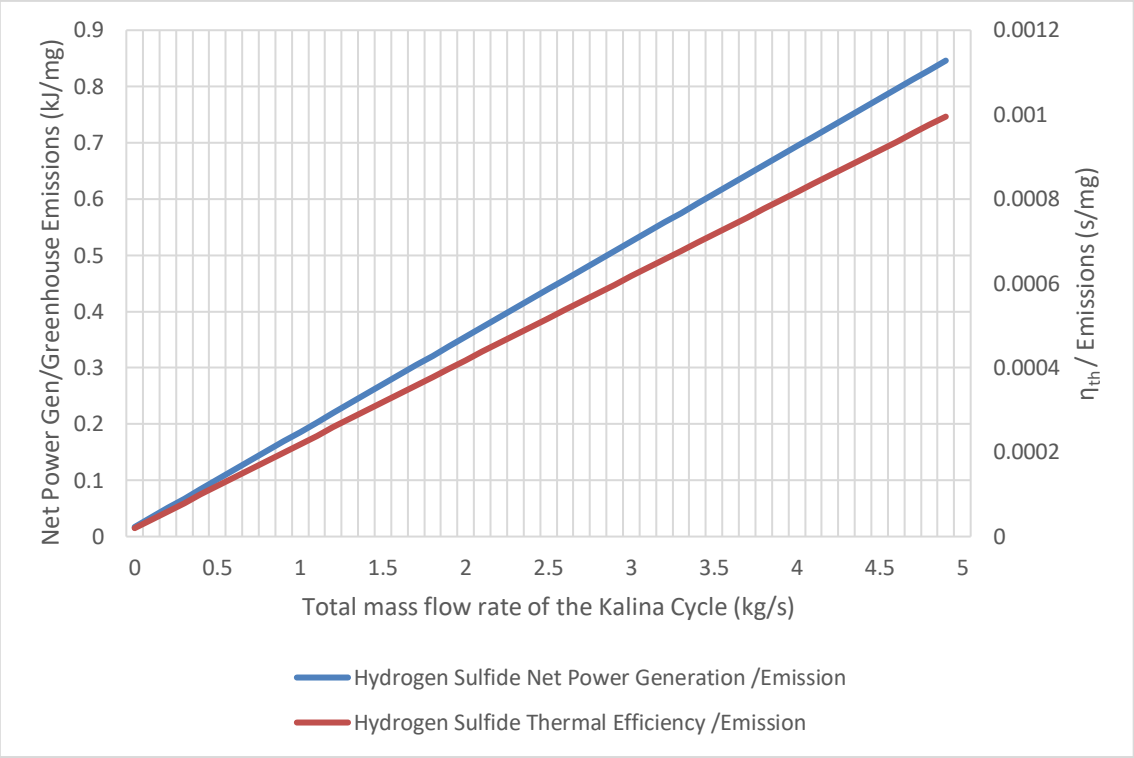


**Figure 6.4:** Variation of net power generation to $H_2S$ emission and thermal efficiency to $H_2S$ emission ratios with respect to total working fluid mass flow rate in the Kalina cycle.

Figure 6.4 shows that both net power output and thermal efficiency per unit of $H_2S$ emission increase as the mass flow rate rises. Since $H_2S$ is produced solely through the AD of food waste, its emission level remains constant, regardless of changes in system output. As a result, although the system's performance increases, the constant emission level causes the output to emission ratio to grow. This trend suggests that the environmental burden of $H_2S$ per unit of energy output decreases as the system scale increases.

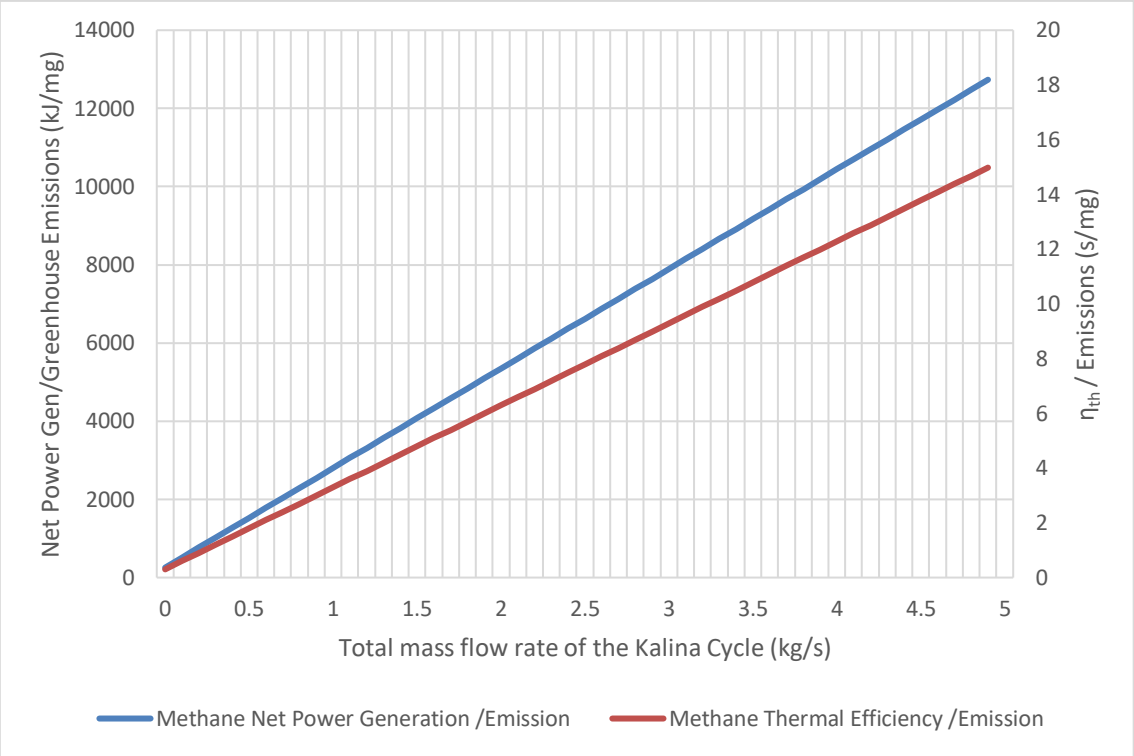


**Figure 6.5:** Variation of net power generation to $CH_4$ emission and thermal efficiency to $CH_4$ emission ratios with respect to total working fluid mass flow rate in the Kalina cycle.

Figure 6.5 shows that both net power output and thermal efficiency per unit of $CH_4$ emission are significantly higher than those observed for other gases. Although methane is generated during the AD of food waste, it is not directly emitted into the atmosphere; instead, it is combusted to provide thermal energy for the cycle. As a result, the amount of $CH_4$ actually emitted to the environment is very low. Because the emission quantity is small, the calculated power and efficiency per unit of $CH_4$ appear high, even when actual system performance is similar to other cases. This highlights methane's dual benefit as both a renewable energy source and a gas with limited environmental release under controlled operation.

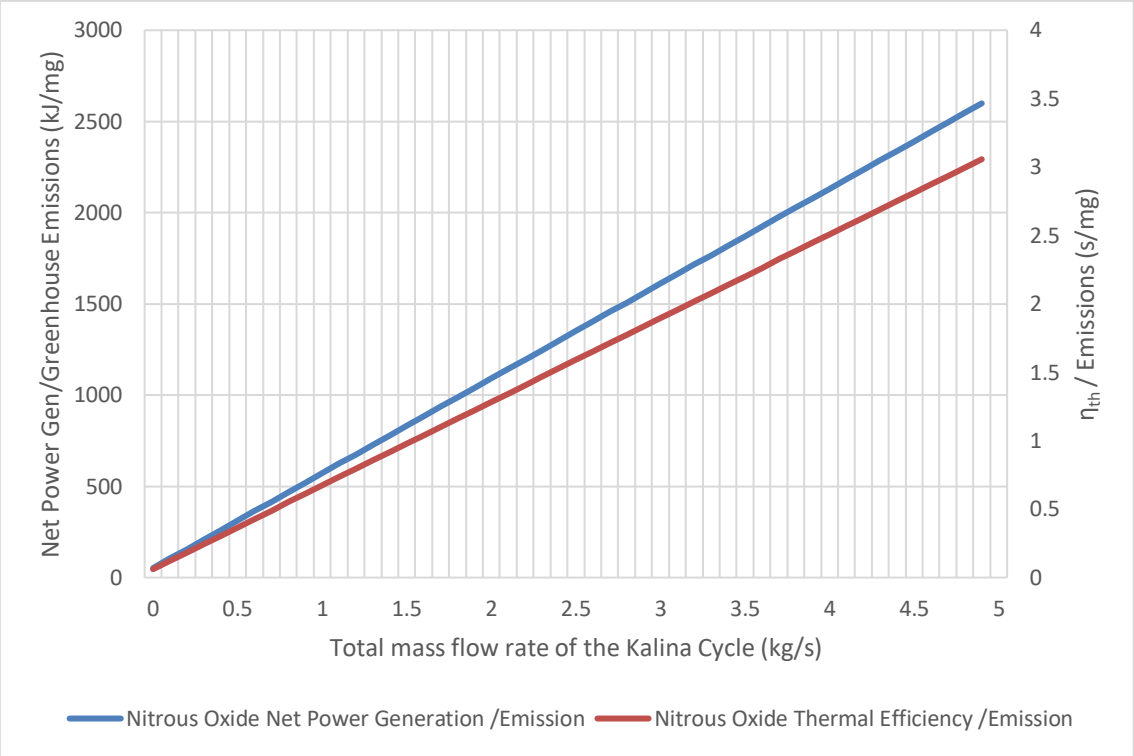


**Figure 6.6:** Variation of net power generation to $N_2O$ emission and thermal efficiency to $N_2O$ emission ratios with respect to total working fluid mass flow rate in the Kalina cycle.

Figure 6.6 indicates that both net power output and thermal efficiency per unit of $N_2O$ emission increase as the mass flow rate rises, but the values are lower than those observed for most other gases. $N_2O$ is produced as a byproduct of methane combustion and does not play a direct role in energy generation. Although the system's overall performance improves with higher flow rates, the amount of $N_2O$ emitted remains significant, which limits the calculated power and efficiency per unit of emission.

### 6.2.2 Effect of Turbine Inlet Temperature

This section analyzes how variations in turbine inlet temperature influence the performance of the KC. The evaluation focuses on changes in net power output and thermal efficiency in response to increasing thermal input conditions.

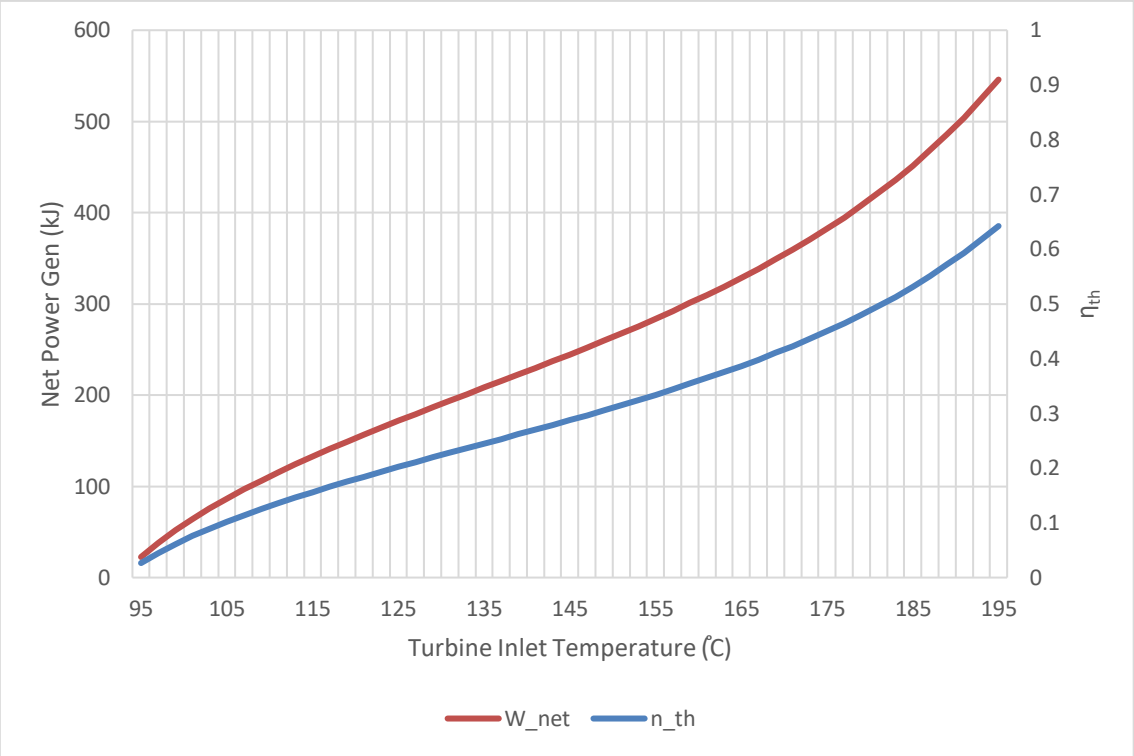


**Figure 6.7:** Variation of net power generation and thermal efficiency with respect to total mass flow rate in the Kalina cycle.

Figure 6.7 presents how turbine inlet temperature influences the net power output and thermal efficiency of the KC. Both performance indicators increase with temperature, although the trend is not strictly linear. While the rate of increase is more significant at lower temperature ranges, it gradually slows down at higher temperatures. This behaviour indicates that the additional gain in performance becomes limited as the system approaches thermodynamic constraints. Net power increases more rapidly because higher inlet temperatures provide greater energy potential, enabling the turbine to generate more mechanical work. In contrast, the rise in thermal efficiency is more moderate, since it depends on both the power produced and the total heat input to the system. These trends suggest that the cycle operates efficiently within a certain temperature range, beyond which the improvements in efficiency diminish.

This general behaviour is also observed in Figures 6.8 through 6.12. This figures express performance indicators in relation to the emission levels of individual gases. This approach provides insight into both the system's energetic behaviour and its environmental performance. Evaluating each emission type individually allows a more

detailed assessment of how turbine inlet temperature influences both energy output and sustainability in relation to emissions.

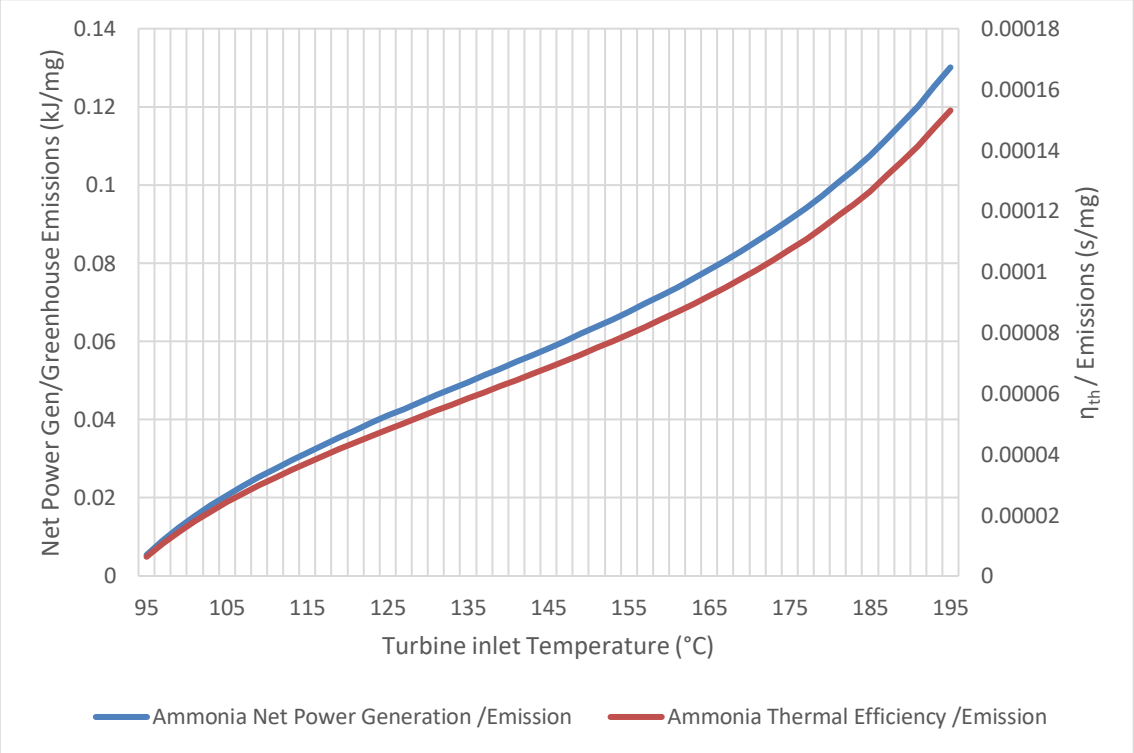


**Figure 6.8:** Variation of net power generation and thermal efficiency per unit $NH_3$ emission with respect to turbine inlet temperature.

In Figure 6.8, both net power output and thermal efficiency per unit of $NH_3$ emission remain low across the temperature range compared to other gases. This is due to the fact that ammonia is not produced during combustion but originates from the AD of nitrogen compounds in food waste. Since the emission rate of $NH_3$ does not significantly change with temperature, the performance indicators per unit of emission improve only slightly, highlighting its weak relation to the system's energy generation process.

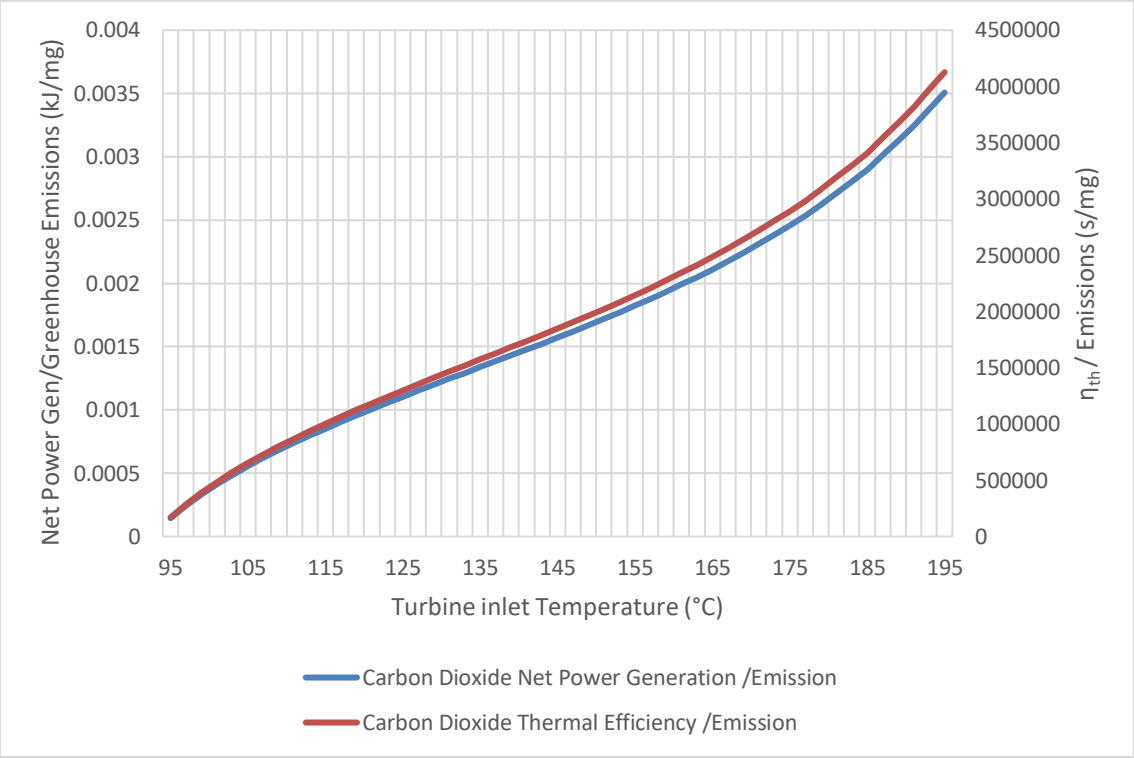


**Figure 6.9:** Variation of net power generation and thermal efficiency per unit $CO_2$ emission with respect to turbine inlet temperature.

In Figure 6.9, both net power output and thermal efficiency per unit of $CO_2$ emission remain lower than those of most other gases across the temperature range. This is because $CO_2$ is released from two separate sources: the AD of food waste and the combustion of $CH_4$. As a result, total $CO_2$ emissions are high, which lowers the calculated power and efficiency per unit of emission. Although the overall cycle performance improves at higher temperatures, the high $CO_2$ emission level continues to limit the output obtained per unit of emission.

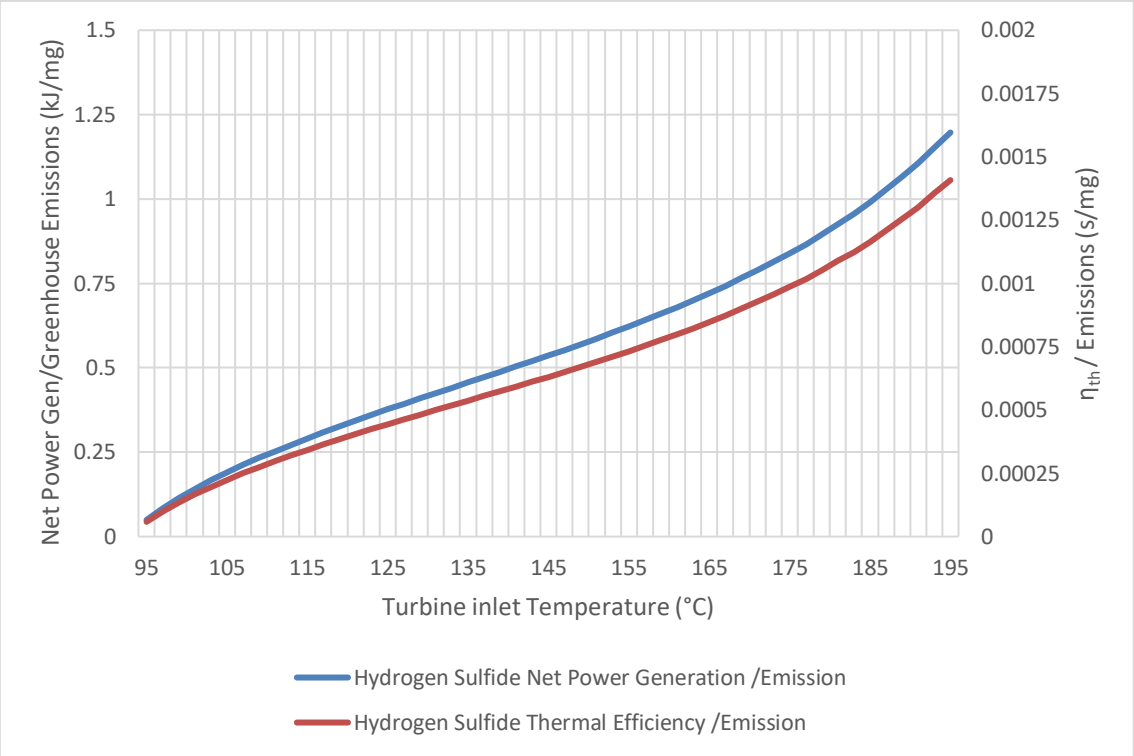


**Figure 6.10:** Variation of net power generation and thermal efficiency per unit $H_2S$ emission with respect to turbine inlet temperature.

Figure 6.10 illustrates a nonlinear increase in both performance indicators with respect to turbine inlet temperature. As temperature rises, both net power generation per unit of $H_2S$ emission and thermal efficiency per unit of $H_2S$ emission exhibit an upward-curving trend. This behavior is attributed to the fact that $H_2S$ emission remains constant while system performance improves with higher temperatures, resulting in progressively higher ratios of performance to emission.

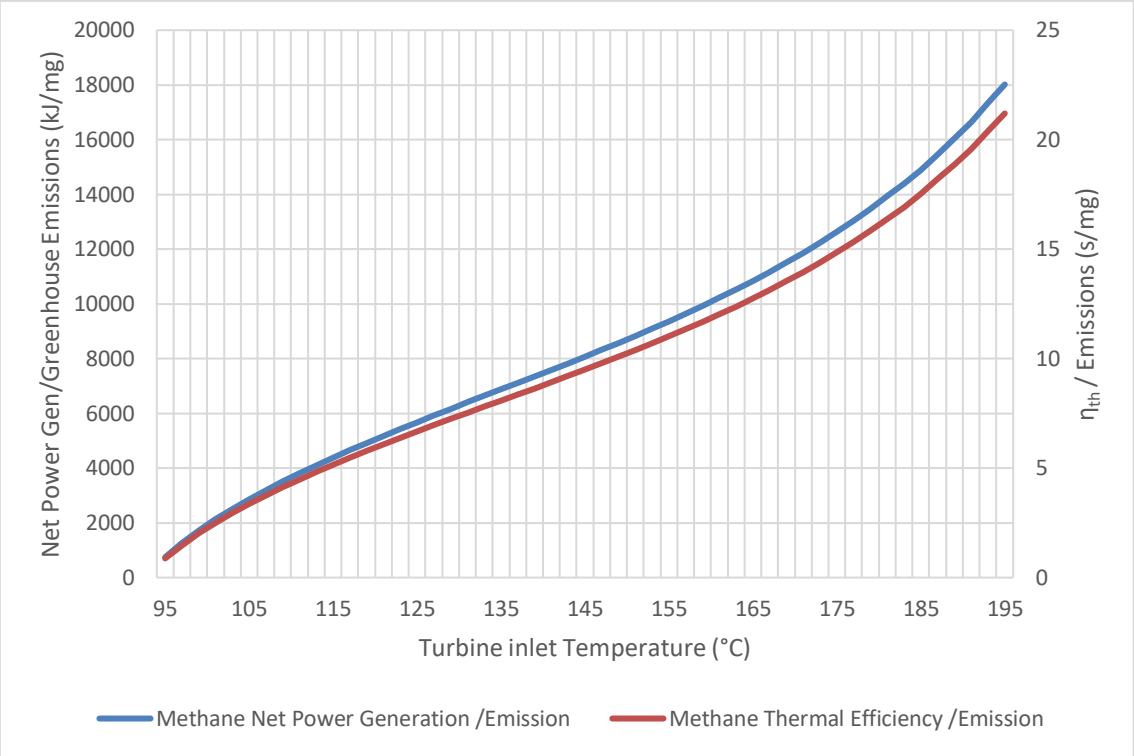


**Figure 6.11:** Variation of net power generation and thermal efficiency per unit $CH_4$ emission with respect to turbine inlet temperature.

Figure 6.11 shows that both performance indicators calculated per unit of $CH_4$ emission increase sharply with rising turbine inlet temperature. This is mainly because $CH_4$ is used as the primary fuel and is almost entirely converted into energy through combustion. As a result, while it contributes significantly to the system's output, only a very small portion is emitted into the atmosphere. The low emission value in the denominator leads to a rapid increase in both indicators as temperature and performance rise.

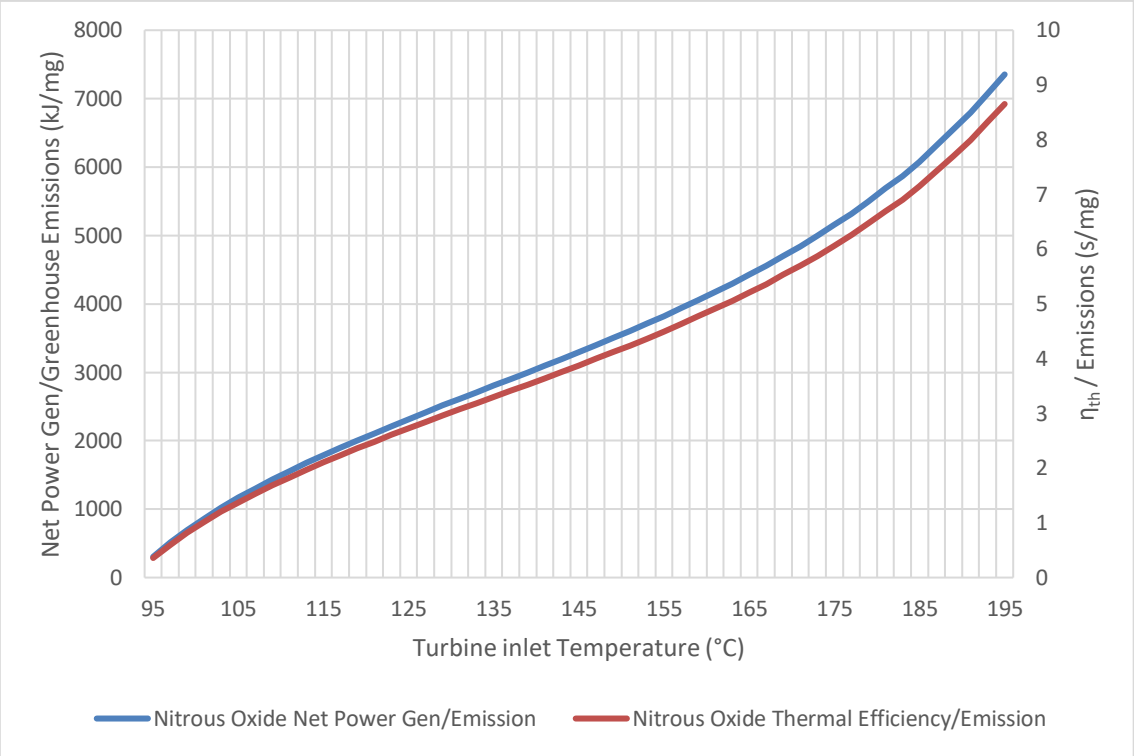


**Figure 6.12:** Variation of net power generation and thermal efficiency per unit $N_2O$ emission with respect to turbine inlet temperature.

Figure 6.12 shows that net power and thermal efficiency per unit of $N_2O$ emission increase with turbine inlet temperature. However, the magnitude of this increase is limited. $N_2O$ is formed during methane combustion and does not contribute to energy production. While the system's performance improves with temperature, $N_2O$ emissions stay constant, which restricts the growth of performance-to-emission ratios.

Methane and nitrous oxide show the highest values of energy output per gram of emission due to their very low release quantities. Methane is almost entirely converted into heat and only a small portion escapes, while $N_2O$ is formed in trace amounts during combustion. Therefore, even moderate increases in energy production lead to high values when considered per unit emission for these gases. In contrast, carbon dioxide is released in large quantities from both digestion and combustion, which reduces the amount of energy produced per gram of $CO_2$. Ammonia and hydrogen sulfide emissions remain constant across all scenarios, so their values are directly proportional to the system's energy performance.

## 6.3 Comparison with Existing Research

These results are consistent with previous work on Kalina Cycle applications. Wang et al. (2019) showed that ammonia–water cycles perform best within a certain range of temperature and flow, which is also confirmed here. However, unlike previous studies, this analysis includes a direct relationship between emissions and energy output, providing a more comprehensive view of system effectiveness. This approach is in line with the methodology introduced by Seçkin (2013), who emphasized the importance of integrating environmental impact into thermodynamic analysis. The inclusion of $CO_2$ capture through calcium looping (Abanades et al., 2007) and catalytic $N_2O$ removal using Co-ZSM-5 (da Cruz et al., 1998) further supports the viability of the system in real-world applications.

## 6.4 Summary

The results show that increasing the mass flow rate and turbine inlet temperature improves both net power generation and thermal efficiency, though gains become limited under extreme operating conditions. When performance is expressed relative to the mass of individual emissions, the system proves especially effective for gases such as $CH_4$ and $N_2O$, which are released in minimal quantities. $CO_2$, with its higher release rate, shows lower values in this context. The inclusion of targeted emission reduction technologies strengthens the environmental feasibility of the KC when used with biomethane as a renewable energy source.

# 7. CONCLUSIONS

This study aimed to evaluate both the energy performance and environmental impact of a KC system fueled by biomethane produced from the AD of food waste. By analyzing variations in working fluid mass flow rate and turbine inlet temperature, the project successfully revealed how key operational parameters influence net power generation, thermal efficiency, and emission output.

One of the major contributions of the study is the coupling of energy analysis with gas-specific emission evaluations. Unlike conventional performance assessments, this approach quantified how much energy is produced relative to the mass of each gas emitted. This provided deeper insight into the environmental effectiveness of the system, especially for methane and nitrous oxide, which exhibited very high energy output per gram of emission due to their minimal release rates. Conversely, carbon dioxide, released in higher amounts, showed lower effectiveness when viewed from this perspective.

The project also included an economic evaluation of greenhouse gas mitigation strategies. Post-combustion $CO_2$ capture via CaL and catalytic decomposition of $N_2O$ using Co-ZSM-5 were analyzed and shown to be technically viable under realistic operating assumptions. These additions strengthen the case for deploying Kalina-based systems in waste-to-energy applications, particularly when emission reduction is a priority.

Overall, the results demonstrate that the KC, when powered by biomethane and supported with emission control technologies, offers a promising solution for low-carbon energy generation. Future work could explore system integration at pilot scale, include dynamic operation scenarios, or extend the model with life cycle and exergy-based sustainability metrics.

# 8. REFERENCES


Incropera, F. P., DeWitt, D. P., Bergman, T. L., & Lavine, A. S. (2007). Fundamentals of Heat and Mass Transfer (6th ed.). John Wiley & Sons.

Abanades, J. C., Grasa, G., Alonso, M., Rodriguez, N., Anthony, E. J., & Romeo, L. M. (2007). Cost structure of a postcombustion $CO_2$ capture system using CaO.

Romeo, L. M., Abanades, J. C., Escosa, J. M., Paño, J., Giménez, A., Sánchez-Biezma, A., & Ballesteros, J. C. (2008). Oxyfuel carbonation/calcination cycle for low cost $CO_2$ capture in existing power plants

Seçkin, C. (2013). "Extended Exergy Accounting (EEA) Analysis of Turkish Society – Determination of Environmental Remediation costs" Phd. Thesis İstanbul Teknik Üniversitesi.

Blamey, J., Anthony, E. J., Wang, J., & Fennell, P. S. (2010). "The calcium looping cycle for large-scale $CO_2$ capture." Progress in Energy and Combustion Science, 36(2), 260–279.

Eurostat (2023). Industrial electricity price statistics. European Commission.

Seçkin, C. 2019, Effect of Operational Parameters on a Novel Combined Cycle of ejector Refrigeration Cycle and Kalina Cycle, Department of Mechanical Engineering, Faculty of Engineering, Marmara University, Turkiye

IPCC. (2006). 2006 IPCC Guidelines for National Greenhouse Gas Inventories, Volume 2: Energy, Chapter 2: Stationary Combustion. Intergovernmental Panel on Climate Change.

Martínez, I., Arias, B., Grasa, G. S., & Abanades, J. C. (2018). $CO_2$ capture in existing power plants using second generation Ca-Looping systems firing biomass in the calciner.

Galle, M., Agar, D. W., & Watzenberger, O. (2001). Thermal $N_2O$ decomposition in regenerative heat exchanger reactors. *Chemical Engineering Science.*

Haber, J., Machej, T., Janas, J., & Nattich, M. (2004). Catalytic decomposition of $N_2O$.

da Cruz, R. S., Mascarenhas, A. J. S., & Andrade, H. M. C. (1998). Co-ZSM-5 catalysts for $N_2O$ decomposition. Applied Catalysis B: Environmental,

Wang, J., Manovic, V., Wu, Y., & Anthony, E. J. (2009). A study on the activity of CaO-based sorbents for capturing $CO_2$ in clean energy processes.

Abanades, J. C. (2002). The maximum capture efficiency of $CO_2$ using a carbonation/calcination cycle of $CaO/CaCO_3$.

Kalina, A.I. (1983) Combined cycle system with novel bottoming cycle. ASME Journal of Engineering for Power, 105(4), 765–771.

Wang, J., Wu, Y., Liu, X. (2019) Thermodynamic and economic analysis of a Kalina cycle-based combined heating and power system for low-temperature heat source utilization. Applied Thermal Engineering, 158, 113755.

Çengel, Y.A., Boles, M.A. (2015) *Thermodynamics: An Engineering Approach*, 8. Baskı, McGraw-Hill Education, New York, USA.

F-Chart Software (2023) *Engineering Equation Solver (EES)*, https://fchartsoftware.com (06.02.2025).

De Clercq, D., Wen, Z., Fan, F., & Caicedo, L. (2016). Biomethane production potential from restaurant food waste in megacities and project level-bottlenecks: A case study in Beijing. Renewable and Sustainable Energy Reviews, 59, 1676–1685.

Engineering ToolBox. (2001). Engineering resources and tools. Retrieved July 8, 2025, from https://www.engineeringtoolbox.com/

# APPENDICES

Screenshots of the code used for thermodynamic modeling and emission calculations. This code was developed and executed in EES to simulate the Kalina Cycle system and assess performance parameters under varying input conditions.

```
"KALINA CYCLE  WITH COMPONENT HEADINGS (STATE POINTS 1-12)"

"INPUT PARAMETERS"
Q_dot_in = 1000 "kW, Heat input to the cycle"    "Total heat provided to the Kalina system."
T9 = 25       "°C, Temperature at state-point 9" "Condenser outlet temperature."
x1 = 0,7       "% ammonia concentration at state-point 1" "Initial ammonia concentration of working fluid."
n_t = 0,8      "Turbine efficiency (%)" "Isentropic efficiency used to calculate actual turbine output."
"T2 = 120  "      "°C, Temperature at state-point 2" "Turbine inlet temperature."
T1 = T2        "Assuming T1 = T2" "HE outlet assumed same as turbine inlet."
T2 = T3        "Assuming T2 = T3" "Same temp for separator branches."
P2 = 3500      "kPa, Pressure at state-point 2" "Operating pressure of turbine and separator."
P1 = P2        "Assuming P1 = P2" "Constant pressure across HE outlet."
P2 = P3        "Assuming P2 = P3" "Same pressure for vapor and liquid branches."
q3 = 0         "Quality at state-point 3, assumed to be 0 (saturated liquid)" "Liquid stream from separator."
q2 = 1         "Quality at state-point 2, assumed to be 1 (saturated vapor)" "Vapor stream from separator."
q9 = 0         "Quality at state-point 9, assumed to be 0 (saturated liquid)" "Condensate after heat rejection."
x1 = x7        "Ammonia concentration at state 1 and 7 are assumed equal" "Mixing fluid composition assumption."
x7 = x8        "Ammonia concentration at state 7 and 8 are assumed equal"
x8 = x9        "Ammonia concentration at state 8 and 9 are assumed equal"
s2 = s6        "Assuming reversible process."
x2 = x6        "Concentration unchanged."
P11 = P4       "Matching pressures."
x11 = x1

n_HE = 0,85     "Heat exchanger efficiency" "Fraction of heat effectively used from Q_dot_in."
Q_dot_1 = Q_dot_in * n_HE  "Heat transfer rate for heat exchanger" "Net heat absorbed by working fluid."
m_dot_1 = 1,98  "kg/s, Mass flow rate of the working fluid" "Main loop mass flow."

"--- CONDENSER ---"
P9 = pressure(NH3H2O; T=T9; q=q9; x=x9) "Calculates pressure for saturated liquid at condenser exit."
P8 = P9
T8 = temperature(NH3H2O; P=P8; x=x8; h=h8)
m_dot_8 = m_dot_1
Q_dot_c = m_dot_8 * (h8 - h9) "Heat rejected to environment."

"--- SEPARATOR ---"
x2 = massfraction(NH3H2O; T=T2; P=P2; q=q2) "Vapor-side ammonia fraction."
x3 = massfraction(NH3H2O; T=T3; P=P3; q=q3) "Liquid-side ammonia fraction."
m_dot_2 = m_dot_6 "Vapor branch flows to turbine."
P9 = P6 "Equalizing pressure across condenser outlet and turbine exit."
m_dot_1 = m_dot_2 + m_dot_3 "Total flow divides into vapor and liquid."
m_dot_1 * x1 = m_dot_2 * x2 + m_dot_3 * x3 "Ammonia mass conservation."
```

```
"--- TURBINE ---"
h2 = enthalpy(NH3H2O; T=T2; P=P2; q=q2) "Inlet enthalpy for turbine."
s2 = entropy(NH3H2O; T=T2; P=P2; q=q2) "Isentropic expansion begins here."
h6_is = enthalpy(NH3H2O; P=P6; x=x6; s=s2) "Isentropic outlet enthalpy."
h6 = h2 - (h2 - h6_is) * n_t "Actual enthalpy using turbine efficiency."
T6 = temperature(NH3H2O; P=P6; x=x6; h=h6) "Turbine outlet temperature."
W_dot_T = m_dot_2 * h2 - m_dot_6 * h6 "Turbine work output."

"--- HEAT ENGINE (HE I) ---"
h3 = enthalpy(NH3H2O; T=T3; P=P3; q=q3) "Separator liquid-side enthalpy."
h1 = enthalpy(NH3H2O; T=T1; P=P1; x=x1) "HE outlet enthalpy."
Q_dot_1 = m_dot_1 * (h1 - h12) "Effective heat input to the cycle."

"--- LTR (Low Temperature Recuperator) ---"
P9 = P7 "Equalizing condenser and LTR pressures."
q7 = quality(NH3H2O; P=P7; x=0,7; s=s6) "Determine phase at inlet."
T7 = temperature(NH3H2O; P=P7; x=0,7; q=0,7) "LTR outlet temp."
h7 = enthalpy(NH3H2O; T=T7; P=P7; x=x7) "LTR outlet enthalpy."
m_dot_7 = m_dot_1 "LTR side flow."
m_dot_3 = m_dot_5 "Branching for HTR."
m_dot_11 * (h11 - h10) = m_dot_7 * (h7 - h8) "Regenerator energy match."


"--- VALVE ---"
h4 = h5 "Isenthalpic throttling."
x3 = x4 "Composition unchanged."
P4 = P2 "Upstream pressure."
T4 = temperature(NH3H2O; P=P4; x=x4; h=h4) "Pre-throttle temp."
P7 = P5 "Post-throttle pressure."
x5 = x4
m_dot_4 = m_dot_5
T5 = temperature(NH3H2O; P=P5; x=x5; h=h5) "Post-throttle temp."

"--- HTR (High Temperature Recuperator) ---"
TTD = 10 "Approach temp diff."
T11 = T7 - TTD "HTR inlet temp."
h11 = enthalpy(NH3H2O; T=T11; P=P11; x=x11) "HTR cold stream inlet enthalpy."
m_dot_11 = m_dot_1
m_dot_11 = m_dot_12
m_dot_3 * (h3 - h4) = m_dot_11 * (h12 - h11) "Energy balance."
```

```
"--- PUMP ---"
h9 = enthalpy(NH3H2O; T=T9; P=P9; x=x9) "Pump inlet enthalpy."
s9 = entropy(NH3H2O; T=T9; P=P9; x=x9)
P10 = P2
x10 = x1
h10_is = enthalpy(NH3H2O; P=P10; x=x10; s=s9)
n_p = 0,6
h10 = h9 - (h9 - h10_is) * n_p "Actual enthalpy rise."
m_dot_9 = m_dot_1
m_dot_9 = m_dot_10
W_dot_pump = m_dot_9 * (h10 - h9) "Pump work required."
T10 = temperature(NH3H2O; P=P10; x=x10; h=h10) "Pump outlet temp."

"--- OVERALL PERFORMANCE ---"
W_net = W_dot_T - W_dot_pump "Net power output."
n_th = W_net/Q_dot_1 "Thermal efficiency."

molc=39,35 [mol]
molh= 70,4 [mol]
molo=25,72 [mol]
moln=2,76 [mol]
mols=0,15 [mol]
carbon_atomic_weight=0,012 [kg]
hydrogen_atomic_weight=0,001 [kg]
oxygen_atomic_weight=0,016 [kg]
nitrogen_atomic_weight=0,014 [kg]
sulfur_atomic_weight=0,032 [kg]

methane_molar_mass=carbon_atomic_weight+4*hydrogen_atomic_weight
carbondioxide_atomic_weight=carbon_atomic_weight+2*oxygen_atomic_weight
water_atomic_weight=2*hydrogen_atomic_weight+oxygen_atomic_weight
ammonia_atomic_weight=nitrogen_atomic_weight+3*hydrogen_atomic_weight
hydrogensulfide_atomic_weight=2*hydrogen_atomic_weight+sulfur_atomic_weight

c=39,35
h=70,4
o=25,72
n=2,76
s=0,15
```

```
H2O=(4*c-h-2*o+3*n+2*s)/4
CO2=(4*c-h+2*o+3*n+2*s)/8
CH4=(4*c+h-2*o-3*n-2*s)/8
NH3=n
H2S=s

methane_HHV= 37,11*(10^6) [J/m^3]
rate_of_heat_transfer=Q_dot_in*10^3 [W]
methane_density= 0,668 [kg/m^3]

methane_vdot =rate_of_heat_transfer/methane_HHV
methane_mdot_buswell=methane_density*methane_vdot
methane_moldot=methane_mdot_buswell/methane_molar_mass

foodwaste_moldot=methane_moldot/20,97
foodwaste_required=foodwaste_moldot/0,6

water_required=foodwaste_required*11,04
carbondioxide_required=foodwaste_required*18,38
ammonia_required=foodwaste_required*2,76
methane_required=foodwaste_required*20,97
hydrogensulfide_required=foodwaste_required*0,15

water_mdot=water_atomic_weight*water_required
carbondioxide_mdot=carbondioxide_atomic_weight*carbondioxide_required
ammonia_mdot=ammonia_atomic_weight*ammonia_required
methane_mdot_real=methane_molar_mass*methane_required
hydrogensulfide_mdot=hydrogensulfide_atomic_weight*hydrogensulfide_required

ammonia_density=0,717
hydrogensulfide_density=1,434
carbondioxide_density=1,842
water_density=997,05

ammonia_vdot=ammonia_mdot/ammonia_density
hydrogensulfide_vdot=hydrogensulfide_mdot/hydrogensulfide_density
carbondioxide_vdot=carbondioxide_mdot/carbondioxide_density
water_vdot=water_mdot/water_density
methane_volumerate=methane_mdot_real/methane_density
```

```
boiler_efficiency=0,98
methane_burned=methane_mdot_real*boiler_efficiency
methane_unburned=0,02*methane_mdot_real
carbon_dioxide_mdot_burned=methane_burned*0,044
carbon_dioxide_burned_emission=2,83*methane_burned

carbon_dioxide_emission_factor=56100 [kg/TJ]
nitrous_oxide_emission_fact=0,1 [kg/TJ]
methane_emission_factor=1 [kg/TJ]

LHV_methane=50,49
methane_burned_emissions=methane_burned*LHV_methane*10^(-6) [kg/s]
methane_unburned_emission=methane_unburned*LHV_methane*10^(-6) [kg/s]
carbondioxide_methane_emission=methane_burned_emissions*carbon_dioxide_emission_factor
nitrous_oxide_emission=methane_burned_emissions*nitrous_oxide_emission_fact
carbondioxide_emission_total=carbondioxide_methane_emission+carbondioxide_mdot

A_1_methane = W_net/methane_unburned_emission*10^(-6)
A_1_carbondioxide = W_net/carbondioxide_emission_total*10^(-6)
A_1_hydrojensulfide = W_net/hydrogensulfide_mdot*10^(-6)
A_1_ammonia = W_net/ammonia_mdot*10^(-6)
A_1_n2o=W_net/nitrous_oxide_emission*10^(-6)

A_2_methane = n_th/methane_unburned_emission*10^(-6)
A_2_carbondioxide = n_th/carbondioxide_emission_total*(10^6)
A_2_hydrojensulfide =n_th/hydrogensulfide_mdot*10^(-6)
A_2_ammonia = n_th/ammonia_mdot*10^(-6)
A_2_n2o=n_th/nitrous_oxide_emission*10^(-6)
```